AD_____

Award Number: DAMD17-03-1-0363

TITLE: Therapeutic Vascular Targeting and Irradiation: Correlation of MRI and Tissue Changes at Cellular and Molecular Levels to Optimizing Outcomes

PRINCIPAL INVESTIGATOR: Dawen Zhao, M.D., Ph.D.

CONTRACTING ORGANIZATION: The University of Texas
Southwestern Medical Center
Dallas, TX 75390

REPORT DATE: June 2004

TYPE OF REPORT: Annual

PREPARED FOR: U.S. Army Medical Research and Materiel Command
Fort Detrick, Maryland 21702-5012

REPORT DOCUMENTATION PAGE

Form Approved
OMB No. 074-0188

1. AGENCY USE ONLY (Leave blank)	2. REPORT DATE	3. REPORT TYPE AND DATES COVERED
	June 2004	Annual (1 Jun 2003 - 31 May 2004)

4. TITLE AND SUBTITLE
Therapeutic Vascular Targeting and Irradiation: Correlation of MRI and Tissue Changes at Cellular and Molecular Levels to Optimizing Outcomes

5. FUNDING NUMBERS
DAMD17-03-1-0363

6. AUTHOR(S)

Dawen Zhao, M.D., Ph.D.

7. PERFORMING ORGANIZATION NAME(S) AND ADDRESS(ES)

The University of Texas
Southwestern Medical Center
Dallas, TX 75390

E-Mail: dawen.zhao@UTSouthwestern.edu

8. PERFORMING ORGANIZATION REPORT NUMBER

9. SPONSORING / MONITORING AGENCY NAME(S) AND ADDRESS(ES)

U.S. Army Medical Research and Materiel Command
Fort Detrick, Maryland 21702-5012

10. SPONSORING / MONITORING AGENCY REPORT NUMBER

11. SUPPLEMENTARY NOTES

Original contains color plates: ALL DTIC reproductions will be in black and white

12a. DISTRIBUTION / AVAILABILITY STATEMENT
Approved for Public Release; Distribution Unlimited

12b. DISTRIBUTION CODE

13. ABSTRACT (Maximum 200 Words)

Vascular targeting agents (VTA) are new types of anticancer drugs that act on existing tumor vasculature, causing vascular disruption, which ultimately leads to extensive ischemic tumor cell death. One major goal of this project is to precisely assess the dynamic changes in vascular perfusion and oxygenation at different time points following VTA in breast tumors. *In vivo* non-invasive MRI approaches observed significant decrease in signal intensity by DCE (dynamic contrast enhanced) MRI and ADC (apparent diffusion coefficient) values by diffusion-weighted MRI at 2hr after an injection of combretastatin A4 phosphate (CA4P) at 30 mg/kg. Most importantly, ^{19}F NMR oximetry showed that tumor oxygenation started to drop significantly at 90 min and became worst at 2hr after the injection, compared to pretreated baseline level. The pO_2 improved significantly 24hr later. These MRI data are comparable to histological and immunohistochemical results showing a significant decrease in perfused vessels detected by Hoechst dye 33342 at 2hr after CA4P. We believe in vivo MRI monitoring of tumor vasculature and oxygenation in response to VTA will be very important to optimize timing for combined VTAs with irradiation. While dynamic contrast MRI indicates vascular shut down, the critical pO_2 measurements are potentially more important.

14. SUBJECT TERMS
Vascular targeting, Magnetic resonance imaging (MRI), pO_2, perfusion irradiation

15. NUMBER OF PAGES
36

16. PRICE CODE

17. SECURITY CLASSIFICATION OF REPORT	18. SECURITY CLASSIFICATION OF THIS PAGE	19. SECURITY CLASSIFICATION OF ABSTRACT	20. LIMITATION OF ABSTRACT
Unclassified	Unclassified	Unclassified	Unlimited

Table of Contents

Background:

Tumor growth, survival and metastasis depend critically on the development of new blood vessels: so called angiogenesis (1, 2). Therefore, extensive research has been focused on developing strategies to suppress angiogenesis. Vascular targeting agents (VTA) are new types of anticancer drugs that act on existing tumor vasculature, causing vascular disruption, which ultimately leads to extensive ischemic tumor cell death (3-5). Tubulin binding agents, *i.e.*, combretastatin A-4-phosphate (CA4P), ZD6126, are one kind of VTAs (4, 5). Promising preclinical studies have shown that such agents selectively caused tumor vascular shutdown and subsequently triggered a cascade of tumor cell death in a broad range of experimental tumors (6, 7). More recently, a combination of VTA with other therapeutic modalities, *e.g.*, radiotherapy or chemotherapy produced synergistic effect (8). Traditional methods for detection of therapeutic response generally rely on a gross decrease in tumor size. Although these methods are useful for assessing response at the end of treatment, little information is available early in the course of treatment. Functional MRI permits non-invasive evaluation of tumor physiology, potentially revealing treatment-induced changes occurring prior to overt changes in tumor size (9, 10). One major goal of this project is to apply *in vivo* noninvasive functional MRI approaches for fully understanding and precisely assessing the dynamic changes in blood perfusion and oxygenation in response to VTA, so that we may predict response and optimize timing for combined VTAs with irradiation.

Body:

In accordance with Statement of Work for Year 1 in this project, I have applied functional MRI approaches including DCE (dynamic contrast enhanced) MRI, BOLD (Blood oxygen level dependent) MR and ^{19}F *FREDOM* (Fluorocarbon Relaxometry using Echo planar imaging for Dynamic Oxygen Mapping) NMR oximetry to extensively studying tumor vasculature and oxygenation in subcutaneous model of 13762 rat breast tumors.

For the untreated control tumors, I designed a novel MRI approach to study potential correlation between tumor vasculature evaluated by ^{1}H DCE, BOLD MRI and tumor oxygenation acquired by ^{19}F *FREDOM* oximetry. A significant correlation was found between changes in tissue pO_2 and BOLD response accompanying oxygen intervention in the total of nine 13762NF breast tumors ($R > 0.9$, 11). However, there was a weak correlation between baseline pO_2 and BOLD response. No correlation was found between transverse relaxation rate R_2^* and pO_2 during respiratory challenge. Furthermore, DCE MRI data (IAUC) showed no correlation with ^{19}F pO_2 or BOLD data (11-13).

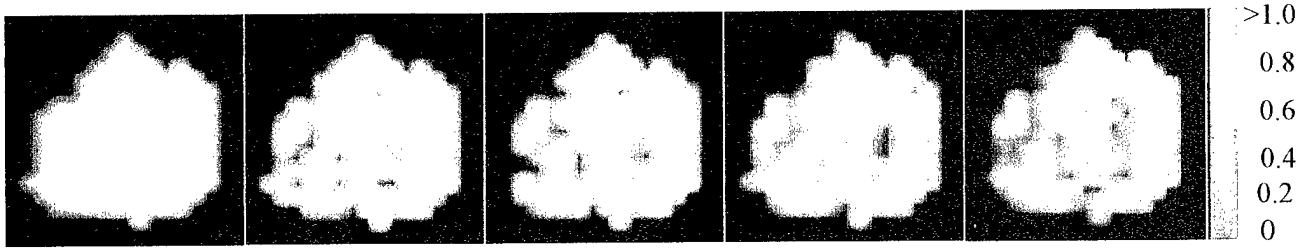

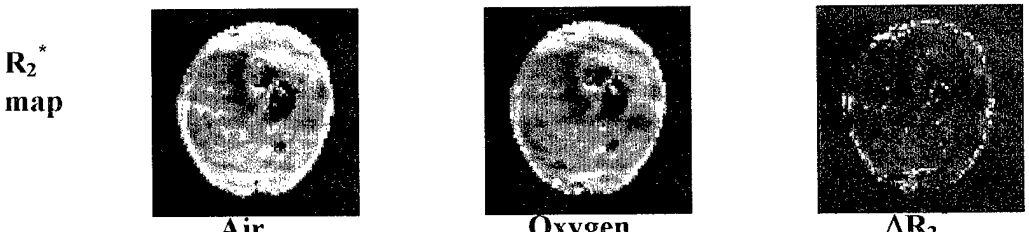

Figure 1 Tumor blood oxygen level dynamics - proton BOLD MRI and R_2^*. A 2 mm slice of a representative breast NF13762 tumor was studied by proton MRI using T_2^*-weighted echo planar imaging (EPI, upper). Normalized subtraction maps at different time points showed heterogeneous response to oxygen inhalation. Significant increase in signal intensity with oxygen breathing indicated decreased deoxyhemoglobin. A maximum 9% increase in mean signal intensity was observed at about 5 min after switching to oxygen. Maps of transverse relaxation rate R_2^* (bottom) were generated from multigradient echo sequence with 8 echoes for the same 2 mm slice. A difference map (ΔR_2^*) by subtracting oxygen map from baseline map showing certain decrease in R_2^* at some tumor regions with respect to oxygen breathing, which is related to decreased deoxyhemoglobin.

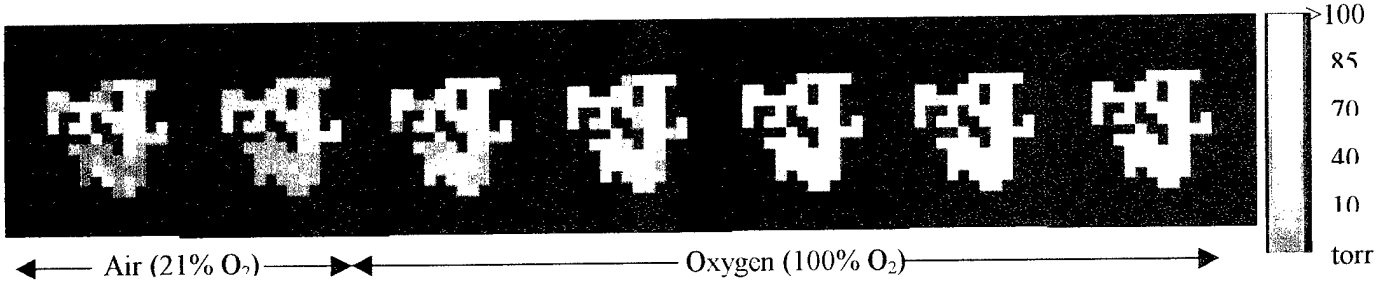

Figure 2 Tumor oximetry – *FREDOM*. ^{19}F pO_2 maps obtained from the 2 mm thick slice of the same tumor, as shown in Figure 1, showed distinct heterogeneity under baseline conditions. Mean pO_2 increased significantly in response to oxygen inhalation, (mean pO_2 = 16 ± 2 (se) vs. 83 ± 7 torr; $p < 0.001$).

I have also performed extensive studies on tumor blood vessels, perfusion, and hypoxia in the 13762 rat breast tumors. Immunohistochemical studies of tumor hypoxia and vasculature using hypoxic marker pimonidazole and endothelium marker CD31 showed that a higher microvascular density (MVD) and lower labeling index of pimonidazole in tumor periphery than the central regions.

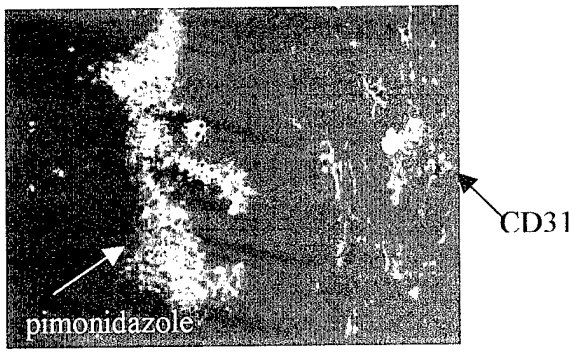

Figure 3 Comparison of pimonidazole and CD31 in a representative tumor. Light immunostaing for CD31 (left) indicated extensive vasculature. Fluorescent staining for hypoxia (pimonidazole, green) was observed at some distance from blood vessels stained for CD31 (red).

Based on the above results, one peer reviewed paper and two abstracts of conference proceeding have been published (11-13), one peer reviewed paper is being prepared (14).

For the treated tumors, integrated functional MRI techniques including ^{1}H Diffusion-weighted MR, DCE MRI and BOLD R_2^* measurements and ^{19}F NMR oximetry were applied to detect early changes in tumor tissue, vasculature and oxygenation after a vascular targeting agent, Combretastatin A4 phosphate (CA4P; OXiGENE, Inc, Waltham, MA) injection. In terms of CA4P dosage, I tried several doses ranging from 30mg/kg to 150mg/kg. My results showed that even a lower dose at 30mg/kg produced significant effect on tumor vasculature. So the dose of 30mg/kg i.p. was used for the whole study. Apparent diffusion coefficient, ADC values obtained by diffusion-weighted MRI showed a significant decrease at 2hr after i.p. CA4P infusion (mean $=1.1 \times 10^{-4}$ versus 0.9×10^{-4} mm^2/sec; $p < 0.01$, Fig. 4). This observation may be interpreted that pre-necrotic process and decrease in blood perfusion cause a decreased extracellular space, which is highly related to proton diffusion distance. For the group of six tumors, there was a general trend with an increase in a mean R_2^* value at 2hr after CA4P (mean = 92.5 ± 7 vs 85.8 ± 6 s^{-1}), but no significant difference was found. Dynamic contrast enhanced MRI demonstrated a significant decrease in IAUC at 2hr after CA4P (0.88 ± 0.06 vs 0.31 ± 0.08, $p < 0.001$), which then recovered to a baseline level at 24hr later (0.82 ± 0.05).

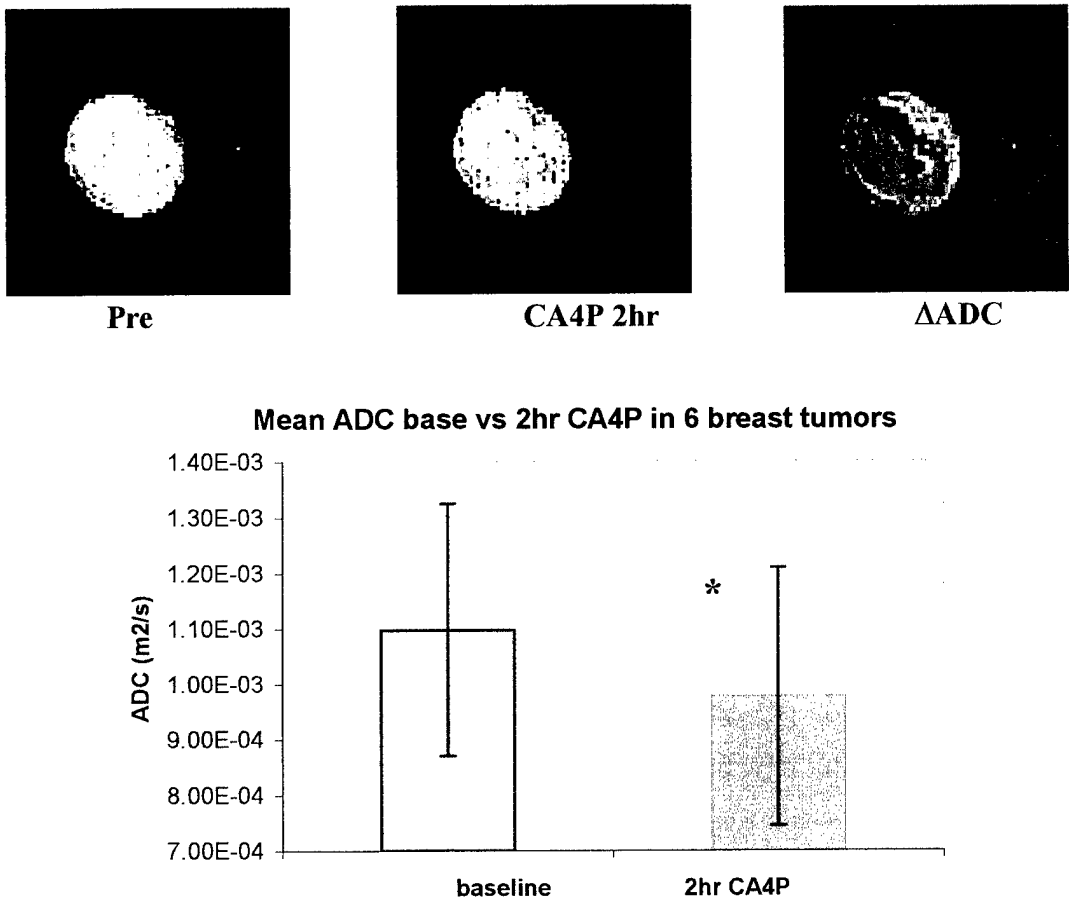

Figure 4 Comparison of ADC values between prior to and after CA4P. Representative ADC maps acquired at pre and 2hr after CA4P and ΔADC map showed decreased ADC value after CA4P. A significant decrease in ADC was found 2hr after i.p. injection of CA4P ($p < 0.01$).

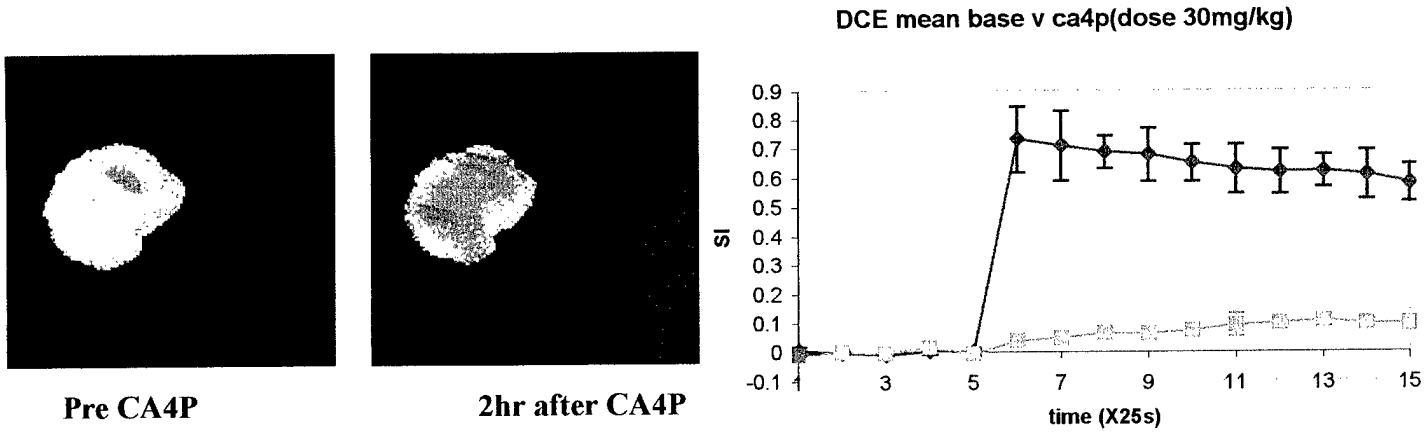

Figure 5 Dynamic contrast enhanced MRI in response to CA4P. Normalized T1-weighted contrast enhanced images were acquired 25 s after a bolus injection of 0.1 mmol/kg Gd-DTPA-BMA at pre and 2hr after i.p. CA4P, respectively. Signal versus time curve showed a significant decrease in signal enhancement (pink) at 2hr after CA4P, compared to that of baseline (blue).

Most interesting and important results obtained by now are data of dynamic tumor oxygenation in response to CA4P because status of tumor oxygen tension is directly related to outcome of irradiation, which has been proposed in Task 2 of this project. To my best knowledge, this study is the first to monitoring tumor pO_2 dynamics following an injection of a VTA agent, which started immediately after injection (10 min) and ended at 24hr after injection. For a group of 7 animals, I found that tumor pO_2 started to drop significantly at 90 min ($pO_2 = 9 \pm 3$ torr) and became worst at 2hr after the injection ($pO_2 = 2 \pm 2$ torr), compared to pretreated baseline level (23 ± 5 torr, $p < 0.01$). In some cases, significant decrease in pO_2 was observed as early as 30 min after injection. The pO_2 improved significantly 24hr later with a mean = 15 ± 4 torr. For the control tumors, there was no significant change in pO_2 after saline injection.

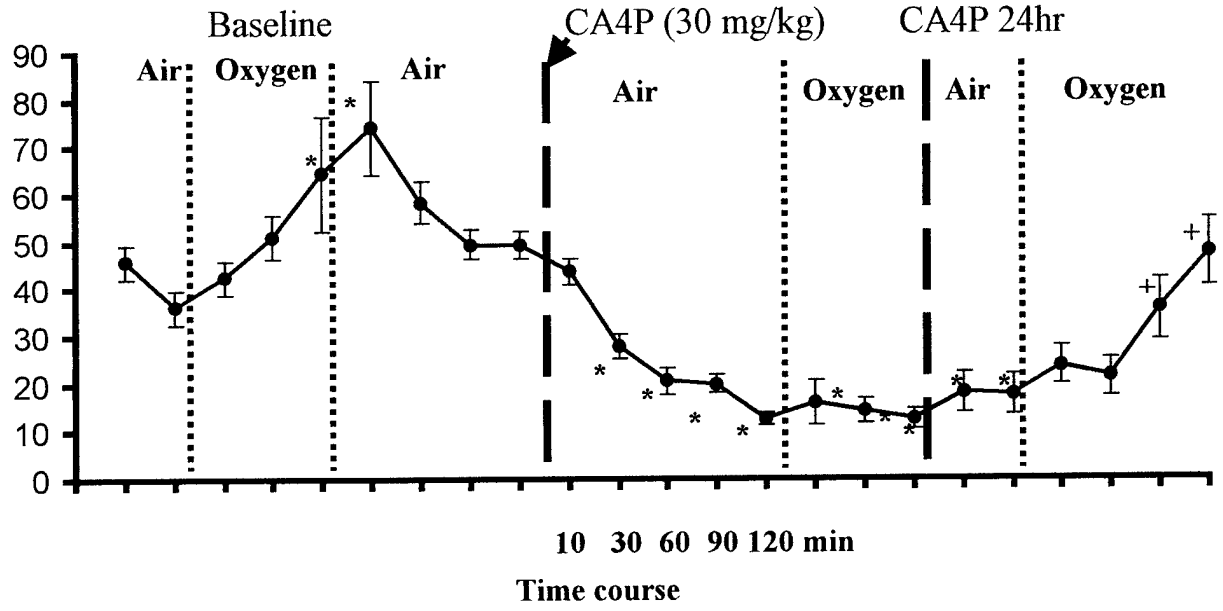

Figure 6 pO_2 (Mean ± SE) obtained from a representative breast tumor in response to CA4P. pO_2 decreased significantly as early as 30 min after injection and dropped to a lowest value at 2hr, and did not respond to oxygen breathing. Despite certain recovery 24 hr later, pO_2 was still significantly lower than the baseline. However, the tumor pO_2 increased significantly to oxygen breathing at this time point ($p < 0.05$). * $p < 0.05$ from baseline air, $^{+}$ $p < 0.05$ from 24hr air.

Such MRI results have been validated by histological and immunohistological studies. Using the perfusion marker, Hoechst 33342 dye, I found a dramatic decrease in fluorescent light density at 2 hr after CA4P, which recovered to some extent at 24 hr.

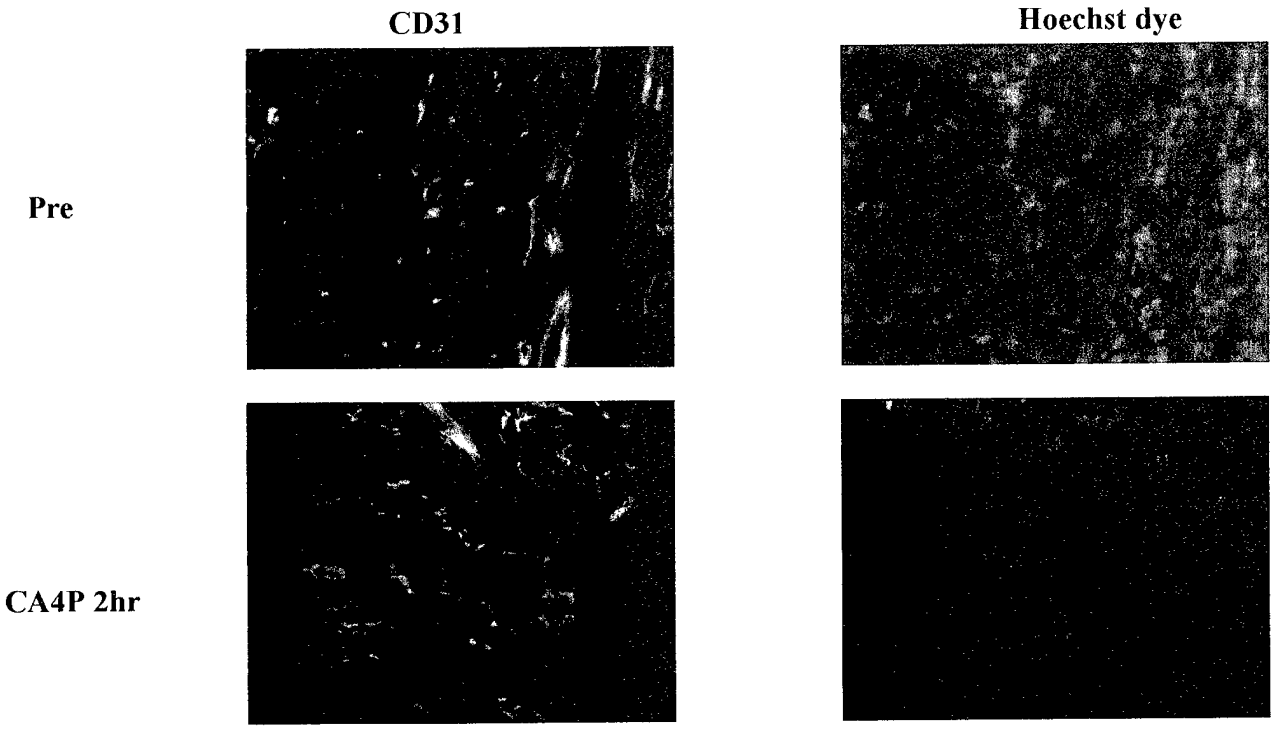

Figure 7 Comparison of tumor perfusion pre and 2hr after CA4P. Fluorescent image showing extensive distribution of vascular endothelium (red) for both tumors (pre and CA4P 2hr). In the same region of each tumor, the number of perfused vessels in the CA4P treated tumor is significantly less than the pretreated tumor.

Based on the CA4P results shown above, two abstracts of conference proceeding and two peer reviewed papers are expected to accomplish. I think such results will be very important for timing combined VTAs with irradiation.

Key Research Accomplishments

- **Assessment of tumor perfusion and oxygenation in the untreated breast tumors by *in vivo* MR approaches**

a. Heterogeneous vasculature and oxygenation within a tumor or between individual tumors has been evaluated in the 13762NF rat breast tumors using integrated proton and fluorine MR techniques.

b. Results of ^{1}H BOLD and DCE MRI, providing information about qualitative vascular oxygenation and perfusion.
c. Significant correlation has been found between changes in tissue pO_2 monitored by ^{19}F NMR oximetry and ^{1}H BOLD response accompanying oxygen intervention.

- **Assessment of dynamic perfusion and oxygenation in the breast tumors in response to a vascular targeting agent, Combretastatin A4 phosphate, by *in vivo* MR approaches**

a. Significant reduction in tumor perfusion was found at early stage of treatment with CA4P (2hr) by ^{1}H DCE MRI and diffusion-weighted MRI.
b. Tumor pO_2 started to drop significantly at 90 min and continued to decrease to a lowest value at 2hr after CA4P.
c. Tumor pO_2 improved at 24hr later, but it was still lower than the pretreated baseline pO_2; pure oxygen inhalation at this time point significantly improved the pO_2, which can be useful in terms of timing for a combination with irradiation in my Task 2 study of this project.

- **Correlation of MR findings with biological studies**

a. Immunohistochemical studies of tumor hypoxia and vasculature using hypoxic marker pimonidazole and endothelium marker CD31 supported our MR findings.
b. Administration of perfusion marker Hoechst dye 33342 showed a significant reduction in perfused vessels at 2hr after CA4P, supporting the MRI results.

Reportable Outcomes

Reportable outcomes that have resulted from this research endeavor include:

- **Peer Reviewed Publications:**

1. **Zhao, D.**, Jiang, L., and Mason, R.P. Measuring changes in tumor oxygenation. *Methods Enzymol.* 386, 378-418, 2004.

- **Abstracts (Published Conference Proceedings):**

Oral presentations:

1. **Zhao, D.**, Jiang, L., Constantinescu, A., Hahn, E.W., and Mason, R.P. Interrogation of tumor vasculature and oxygenation by integrated ^{1}H and ^{19}F MRI. *51st Radiat. Res. Soc.* St. Louis, MO, Apr 2004.
2. **Zhao, D.**, Jiang, L., Constantinescu, A., Hahn, E.W., and Mason, R.P. Evaluation of breast tumor microcirculation and oxygenation using a combination of BOLD, DCE and ^{19}F MRI. *11th ISMRM,* #222, Kyoto, Japan, May 2004.

- **Manuscripts in preparation:**

Abstracts of conference proceeding:

1. **Zhao, D.**, Jiang, L., Adam, A., Hahn, E.W., and Mason, R.P. Evaluation of early change in tumor perfusion and oxygenation in response to vascular targeting agent Combretastatin A4 phosphate by magnetic resonance imaging *in vivo.* 96th AACR. Anaheim, CA.

Peer reviewed papers:

1. **Zhao, D.**, Jiang, L., Hahn, E.W., and Mason, R.P. Evaluation of breast tumor microcirculation and oxygenation using a combination of BOLD, DCE and ^{19}F MRI. *Magn. Reson. Med.*

2. **Zhao, D.**, Jiang, L., Adam, A., Hahn, E.W., and Mason, R.P. Evaluation of early change in tumor perfusion and oxygenation in response to vascular targeting agent Combretastatin A4 phosphate by magnetic resonance imaging *in vivo. Cancer Res.*
3. **Zhao, D.**, Jiang, L., Hahn, E.W., and Mason, R.P. Early tumor response to vascular targeting agent Combretastatin A4 phosphate by diffusion-weighted MRI and dynamic contrast enhanced MRI. *J. Magn. Reson. Imaging.*

- **Employment or research opportunity:**

  Ammar Adam, an experienced research technician, has been recently recruited as a Research Assistant by our department. Mr. Adam will contribute 40% of his effort to this project.

Conclusion:

Results reported here were successful in terms of the outlined tasks cited in the original proposed statement of work. Three publications have been achieved during the Year 1. More importantly, in terms of dosing and timing, the results of Year 1 will lay foundation for the combination treatment of vascular targeting agent with irradiation in the following Task 2 project. Especially, the results of tumor oxygen dynamics following the vascular targeting agent have not been reported before. While dynamic contrast MRI indicates vascular shut down, the critical pO_2 measurements are potentially more important. I am confident that integrated functional MR approaches will facilitate us to fully understand and precisely assess the treatment-induced changes occurring prior to overt changes in tumor size in breast tumors, so that we may predict response and optimize the therapy.

References:

1. Folkman, J. Tumor angiogenesis, Adv. Cancer Res. *19:* 331-58, 1974.
2. Folkman, J. Anti-angiogenesis: new concept for therapy of solid tumors, Ann. Surg. *175:* 409-416, 1972.
3. Denekamp, J. Vasculature as a target for tumor therapy. Prog. Appl. Microcirc. *4:* 28-38, 1986.
4. Chaplin, D. J. and Dougherty, G. J. Tumor vasculature as a target for cancer research, Br. J. Cancer. *80:* 57-64, 1999.S
5. Siemann, D. W., H., W. K., and Horsman, M. R. Targeting tumor blood vessels: an adjuvant strtegy for radiation therapy, Radiother. Oncol. *57:* 5-12, 2000.
6. Chaplin, D. J., Pettit, G. R., and Hill, S. A. Anti-vascular approaches to solid tumor therapy: evaluation of combretastatin A4 phosphate, Anticancer Res. *19:* 189-95, 1999.
7. Davis PD, Dougherty GJ, Blakey DC, et al. ZD6126: a novel vascular-targeting agent that causes selective destruction of tumor vasculature. Cancer Res. *62:* 7247-53, 2002.

8. Siemann, D. W. and Rojiani, A. M. Enhancement of radiation therapy by the novel vascular targeting agent ZD6126, Int. J. Radiat. Oncol. Biol. Phys. *53:* 164-71, 2002.

9. Evelhoch, J. L., Gillies, R. J., Karczmar, G. S., Koutcher, J. A., Maxwell, R. J., Nalcioglu, O., Raghunand, N., Ronen, S. M., Ross, B. D., and Swartz, H. M. Application of magnetic resonance in model systems: cancer therapeutics, Neoplasia. *152:* 152-65, 2000.

10. Gillies RJ, Bhujwalla ZM, Evelhoch J, et al. Applications of magnetic resonance in model systems: tumor biology and physiology. Neoplasia. *2*: 139-51, 2000.

11. **Zhao, D**., Jiang, L., Constantinescu, A., Hahn, E.W., and Mason, R.P. Evaluation of breast tumor microcirculation and oxygenation using a combination of BOLD, DCE and ^{19}F MRI. *11th ISMRM,* #222, Kyoto, Japan, May 2004.

12. **Zhao, D**., Jiang, L., Constantinescu, A., Hahn, E.W., and Mason, R.P. Interrogation of tumor vasculature and oxygenation by integrated ^{1}H and ^{19}F MRI. *51st Radiat. Res. Soc.* St. Louis, MO, Apr 2004.

13. **Zhao, D**., Jiang, L., and Mason, R.P. Measuring changes in tumor oxygenation. *Methods Enzymol.* 386, 378-418, 2004.

Appendices

Methods in Enzymology

Volume 386

Imaging in Biological Research

Part B

EDITED BY

P. Michael Conn

OREGON NATIONAL PRIMATE RESEARCH CENTER
OREGON HEALTH AND SCIENCE UNIVERSITY
BEAVERTON, OREGON

ELSEVIER
ACADEMIC
PRESS

AMSTERDAM • BOSTON • HEIDELBERG • LONDON
NEW YORK • OXFORD • PARIS • SAN DIEGO
SAN FRANCISCO • SINGAPORE • SYDNEY • TOKYO

Academic Press is an imprint of Elsevier

results exhibit a linear correlation between ΔHbO and ΔpO_2 of the tumors under hyperoxic gas intervention, suggesting that the NIRS approach could have a good potential value in the clinic. Finally, the newly developed tumor hemodynamic model allows us to reveal tumor heterogeneities at different tumor locations based on the multichannel NIRS results. Through this chapter, we lay a foundation for an NIR imaging technique to be further developed to facilitate investigations of tumor heterogeneity and vascular perfusion. Such a noninvasive imaging approach can enhance our understanding of the dynamics of tumor oxygenation and the mechanism of tumor physiology under baseline and perturbed conditions.

Acknowledgments

This work was supported in part by the Department of Defense Breast Cancer Research grants BC990287 (HL) and BC000833 (YG), and NIH R01 CA79515 (NCI)/EB002762 (NIBIB) (RPM). We are grateful to Vincent Bourke for his collaborative work on multichannel pO_2 measurements and Dr. Anca Constantinescu for her assistance with all the tumor investigations. We also gratefully acknowledge Dr. Britton Chance for his technical support on the multichannel NIR system.

[18] Measuring Changes in Tumor Oxygenation

By DAWEN ZHAO, LAN JIANG, and RALPH P. MASON

Introduction

Significance of pO_2 in Oncology

It has long been appreciated that hypoxic tumor cells are more resistant to radiotherapy.[1] Indeed, a 3-fold increase in radio resistance may occur when cells are irradiated under hypoxic conditions compared with oxygen pressure $pO_2 > 15$ torr for a given single radiation dose. However, recent modeling has indicated that the proportion of cells in the range 0–20 torr may be most significant in terms of surviving a course of fractionated radiotherapy.[2] Certain chemotherapeutic drugs also present differential efficacy, depending on hypoxia.[3,4] Increasingly, there is evidence that hypoxia also

[1] L. Gray, A. Conger *et al.*, *Br. J. Radiol.* **26,** 638 (1953).
[2] B. G. Wouters and J. M. Brown, *Radiat. Res.* **147,** 514 (1997).
[3] B. Teicher, J. Lazo *et al.*, *Cancer Res.* **41,** 73 (1981).
[4] A. C. Sartorelli, *Cancer Res.* **48,** 775 (1988).

0076-6879/04 $35.00

influences such critical characteristics as angiogenesis, tumor invasion, and metastasis.[5–8] Moreover, repeated bouts of intermittent hypoxic stress may be important in stimulating tumor progression.[9] Thus the ability to measure pO_2 noninvasively and repeatedly, with respect to acute or chronic interventions, becomes increasingly important.

Early work examined cells *in vitro*, where ambient oxygen concentrations are readily controlled. *In vivo*, hypoxia may be achieved by clamping the blood supply to a tumor,[10] but other levels of oxygenation reflect the interplay of supply and consumption.[11,12] Robust fine-needle polarographic electrodes opened the possibility of measuring pO_2 in tumors *in situ* and *in vivo* to define local pO_2 under baseline conditions or with respect to interventions. In early work, Cater and Silver[13] showed the ability to monitor pO_2 at individual locations in patients' tumors with respect to breathing oxygen. Later, Gatenby *et al.*[14] showed that pO_2 in a tumor was correlated with clinical outcome. Tumor oximetry received its greatest boost with the development of the Eppendorf Histograph polarographic needle electrode system.[15] This computer-controlled device equipped with a stepper motor can reveal distributions of tumor oxygenation and has been applied extensively to clinical trials. Many reports have now shown that tumors are highly heterogeneous and have extensive hypoxia; furthermore, strong correlations have been shown in cervix and head and neck tumors between median pO_2 or hypoxic fraction and survival or disease-free survival.[5,16–20] Extensive hypoxia also has been found in tumors of the prostate and breast.[21–23] Thus tumor oxygenation is now recognized as a strong

[5] E. K. Rofstad, K. Sundfor *et al.*, *Br. J. Cancer* **83,** 354 (2000).
[6] K. De Jaeger, M. C. Kavanagh *et al.*, *Br. J. Cancer* **84,** 1280 (2001).
[7] M. Höckel and P. Vaupel, *J. Natl. Cancer Inst.* **93,** 266 (2001).
[8] H. J. Knowles and A. L. Harris, *Breast Cancer Res.* **3,** 318 (2001).
[9] R. A. Cairns, T. Kalliomaki *et al.*, *Cancer Res.* **61,** 8903 (2001).
[10] J. Moulder and S. Rockwell, *Int. J. Radiat. Oncol. Biol. Phys.* **10,** 695 (1984).
[11] T. W. Secomb, R. Hsu *et al.*, *Adv. Exp. Med. Biol.* **454,** 629 (1998).
[12] M. W. Dewhirst, B. Klitzman *et al.*, *Int. J. Cancer* **90,** 237 (2000).
[13] D. Cater and I. Silver, *Acta Radiol.* **53,** 233 (1960).
[14] R. A. Gatenby, H. B. Kessler *et al.*, *Int. J. Radiat. Oncol. Biol. Phys.* **14,** 831 (1988).
[15] M. Nozue, I. Lee *et al.*, *J. Surg. Oncol.* **66,** 30 (1997).
[16] D. M. Brizel, S. P. Scully *et al.*, *Cancer Res.* **56,** 941 (1996).
[17] M. Höckel, K. Schlenger *et al.*, *Cancer Res.* **56,** 4509 (1996).
[18] M. Nordsmark, M. Overgaard *et al.*, *Radiother. Oncol.* **41,** 31 (1996).
[19] A. W. Fyles, M. Milosevic *et al.*, *Radiother. Oncol.* **48,** 149 (1998).
[20] T. H. Knocke, H. D. Weitmann *et al.*, *Radiother. Oncol.* **53,** 99 (1999).
[21] P. W. Vaupel, K. Schlenger *et al.*, *Cancer Res.* **51,** 3316 (1991).
[22] P. Hohenberger, C. Felger *et al.*, *Breast Cancer Res. Treat.* **48,** 97 (1998).
[23] B. Movsas, J. D. Chapman *et al.*, *Urology* **53,** 11 (1999).

prognostic indicator, and this device has laid a convincing foundation for the value of measuring pO_2 in patients. However, the Histograph is highly invasive, and it is not possible to make repeated measurements at individual locations, precluding dynamic studies to assess the influence of interventions on tumor pO_2.

Given that hypoxic tumors are more resistant to certain therapies, it becomes important to assess tumor oxygenation as part of therapeutic planning. Patients could be stratified according to baseline hypoxia to receive adjuvant interventions designed to modulate pO_2, or more intense therapy as facilitated by intensity modulated radiation therapy (IMRT). Tumors, which do not respond to interventions, may be ideal candidates for hypoxia-selective cytotoxins (e.g., tirapazamine[24]). Noting that any therapy and intervention may have side effects or simply add to clinical costs, it is vital that efficacy be established and therapy be optimized for an individual patient. Whether initially hypoxic regions of a tumor can be modified to become better oxygenated has long been considered a key to improving outcome of irradiation. However, many attempts to improve therapeutic outcome by manipulation of tumor oxygenation have shown only modest success in the clinic,[25] and it is thought that lack of success may have resulted from inability to identify those patients who would benefit from adjuvant interventions.

Although pO_2 determinations could be of great clinical value, they are also vital to many laboratory investigations of new drugs and studies of tumor development. Given the potential importance of measuring pO_2, many diverse techniques have been developed, as reviewed by others previously,[26–29] and here, in the next section.

Methods of Measuring Tumor Oxygenation

Table I lists various techniques that have been reported to provide quantitative estimates of pO_2. Historically, polarographic needle oxygen electrodes have been considered a "gold standard," and they have been applied in the clinic since the 1950s. One or more electrodes may be placed in a tumor, facilitating measurement of baseline pO_2 and dynamic response to

[24] J. M. Brown, *Mol. Med. Today* **6,** 157 (2000).
[25] J. Overgaard and M. R. Horsman, *Semin. Radiat. Oncol.* **6,** 10 (1996).
[26] H. B. Stone, J. M. Brown *et al.*, *Radiat. Res.* **136,** 422 (1993).
[27] R. P. Mason, S. Ran *et al.*, *J. Cell. Biochem.* **87S,** (2002).
[28] H. M. Swartz, *Biochem. Soc. Trans.* **30,** 248 (2002).
[29] H. M. Swartz and J. F. Dunn, *in* "Oxygen Transport to Tissue XXIV" (J. F. Dunn and H. M. Swartz, eds.), Vol. 530, p. 1. Kluwer Academic, New York, 2003.

interventions.[13,30–32] Initially, the focus was on generating finer needles, which would be less invasive, and tips as fine as a few microns have been applied to animal tissues.[33] However, such needles are progressively brittle and generate such small current that stray electromagnetic fields can interfere. Stationary electrodes sample limited volumes, and recognizing tumor heterogeneity, the Eppendorf Histograph was developed to generate multiple measurements along tracks in tumors.[15,34,35] Following extensive studies in animals, the Histograph has found widespread application in the clinical setting and has unequivocally revealed hypoxia in many tumor types, for example, head and neck,[36,37] cervix,[19,38] breast,[21,22] and prostate.[23] Moreover, pO_2 distributions have been found to have prognostic value. Disease-free survival is significantly worse for patients with hypoxic tumors, though the optimal prognostic parameter has variously been median pO_2 or percent measurements <5 torr (HF_5).

Although the Eppendorf Histograph uses a large invasive needle (size = 26 G or about 0.35 mm), it has provided great impetus for further investigations. One aspect is the application of less invasive probes. Fiber-optic probes are typically finer and do not consume oxygen during measurement. Typically, only two or four locations are sampled simultaneously, but as with the earlier electrodes, these optical probes facilitate observation of dynamic changes in pO_2 in response to interventions.[39–43] Both the current commercial systems, the OxyLite (http://www.oxford-optronix.com/tissmon/oxylite/oxylite.htm) and FOXY (http://www.oceanoptics.com/Products/foxyfaqs.asp), exploit the fluorescent quenching by oxygen of a ruthenium complex coating. OxyLite measures fluorescent lifetime, whereas FOXY uses a simple intensity integration and is correspondingly much cheaper. Fibers are fragile, and coatings have a limited lifetime.

[30] N. Evans and P. Naylor, *Br. J. Radiol.* **36,** 418 (1963).
[31] C. Song, I. Lee *et al.*, *Cancer Res.* **47,** 442 (1987).
[32] D. Zhao, A. Constantinescu *et al.*, *Int. J. Radiat. Oncol. Biol. Phys.* **53,** 744 (2002).
[33] D. W. Crawford and M. A. Cole, *J. Appl. Physiol.* **58,** 1400 (1985).
[34] F. Kallinowski, R. Zander *et al.*, *Int. J. Radiat. Oncol. Biol. Phys.* **19,** 953 (1990).
[35] P. W. Vaupel, D. K. Kelleher, and M. Günderoth, "Tumor Oxygenation." Gustav Fischer Verlag, Stuttgart, Germany, 1995.
[36] D. M. Brizel, G. S. Sibly *et al.*, *Int. J. Radiat. Oncol. Biol. Phys.* **38,** 285 (1997).
[37] V. Rudat, B. Vanselow *et al.*, *Radiother. Oncol.* **57,** 31 (2000).
[38] C. Aquino-Parsons, A. Green *et al.*, *Radiother. Oncol.* **57,** 45 (2000).
[39] J. R. Griffiths, *Br. J. Radiol.* **72,** 627 (1999).
[40] J. Bussink, J. H. A. M. Kaanders *et al.*, *Radiat. Res.* **154,** 547 (2000).
[41] R. D. Braun, J. L. Lanzen *et al.*, *Am. J. Physiol. Heart Circ. Physiol.* **280,** H2533 (2001).
[42] D. Zhao, A. Constantinescu *et al.*, *Am. J. Clin. Oncol.* **24,** 462 (2001).
[43] Y. Gu, V. Bourke *et al.*, *Appl. Opt.* **42,** 1 (2003).

TABLE I
TUMOR OXIMETRY METHODS

Technique	Reporter	Parameter measured	Invasiveness	Characteristic resolution: Spatial	Characteristic resolution: Temporal	References
FREDOM	HFB	R_1	Minimal 32-G needle	Map multiple locations each 8 mm^3	6.5 min	Hunjan, Zhao *et al.*[159]; Zhao, Constantinescu *et al.*[134]; Song, Constantinescu *et al.*[135]; Zhao, Constantinescu *et al.*[32]; Kim, Zhao *et al.*[106]; Zhao, Constantinescu *et al.*[136]; Zhao, Ran *et al.*[137]
^{19}F MRI	PFC	R_1	IV	Perfused regions	min	Hees and Sotak[153]; Dardzinski and Sotak[117]; McIntyre, McCoy *et al.*[158]; Fan, River *et al.*[95]; Wang, Su *et al.*[88]
^{19}F MRS	PFC	R_1	IV	Perfused regions	s to min	Hees and Sotak[153]; Mason, Antich *et al.*[154]; Baldwin and Ng[156]; McIntyre, McCoy *et al.*[158]; van der Sanden, Heerschap *et al.*[138]
DCE MRI	Gd-DTPA	Contrast kinetics	IV	Maps	min	Cooper, Carrington *et al.*[87]; Lyng, Vorren *et al.*[a]; Wang, Su *et al.*[88]
ESR/EPR	Charcoal, phthalocyanine	Linewidth	Needle	Single location 23 G IT	seconds	O'Hara, Goda *et al.*[b]; Goda, Bacic *et al.*[c]; O'Hara, Goda *et al.*[59]; Gallez, Jordan *et al.*[d]; Jordan, Misson *et al.*[48]; He, Beghein *et al.*[49]; Jiang, Beghei *et al.*[50]; O'Hara, Blumenthal *et al.*[e]; Baudelet and Gallez[94]; Dunn, O'Hara *et al.*[f]; Jordan, Gregoire *et al.*[52]; Mahy, De Bast *et al.*[55]
ESR/EPR	Nitroxides	Linewidth	IV	Global or map	s to min	Elas, Williams *et al.*[53]
OMRI	Free radical	Overhauser enhancement	IV	mm^3 maps	10 min	Krishna, English *et al.*[60]
Needle electrode	Oxygen	Current	Needle 26 G IT	Single location	~1 s	Cater and Silver[13]; Evans and Naylor[30]; Hasegawa, Rhee *et al.*[g]; Gatenby, Kessler *et al.*[14]; Song, Shakil *et al.*[h]; Zhao, Constantinescu *et al.*[32]
(Histograph)	Oxygen	Current	Needle 26 G IT	Multiple tracks	1 s per location	Eble, Wenz *et al.*[i]; Falk, Laurence *et al.*[j]; Vaupel, Kelleher *et al.*[35]; Brizel, Scully *et al.*[16]; Höckel, Schlenger *et al.*[k]; Nozue, Lee *et al.*[15]; Fyles, Milosevic *et al.*[19]; Siemann, Johansen *et al.*[l]; Mason, Constantinescu *et al.*[175]; Aquino-Parsons, Green *et al.*[38]; Jenkins, Evans *et al.*[75]; Höckel and Vaupel[7]

(continued)

TABLE I *(continued)*

Technique	Reporter	Parameter measured	Invasiveness	Characteristic resolution: Spatial	Characteristic resolution: Temporal	References
Optical probe (OxyLite, FOXY)	Rh complex	Fluorescent lifetime	Needle (26 G)	2–4 locations	Real time	Griffiths[39]; Bussink, Kaanders *et al.*[40]; Braun, Lanzen *et al.*[41]; Zhao, Constantinescu *et al.*[134]; Gu, Bourke *et al.*[43]; Jordan, Beghein *et al.*[54]
Phosphorescence	PD complex	Lifetime	IV	Maps	<1 min	Wilson[m]; Vinogradov, Lo *et al.*[n]; Dewhirst, Ong *et al.*[o]; Wilson, Vinogradov *et al.*[63]; Erickson, Braun *et al.*[p]
Fluorescence	EF5	Fluorescent intensity	IV + biopsy	Maps microscopic	Once	Koch[79]
Mass spectrometry	Oxygen	Atoms	Needle	Single location		Potapov, Sirovskii *et al.*[q]

[a] H. Lyng, A. O. Vorren *et al.*, *J. Magn. Reson. Imaging* **14,** 750 (2001).
[b] J. A. O'Hara, F. Goda *et al.*, *Radiat. Res.* **144,** 222 (1995).
[c] F. Goda, G. Bacic *et al.*, *Cancer Res.* **56,** 3344 (1996).
[d] B. Gallez, B. F. Jordan *et al.*, *Magn. Reson. Med.* **42,** 627 (1999).
[e] J. A. O'Hara, R. D. Blumenthal *et al.*, *Radiat. Res.* **155,** 466 (2001).
[f] J. F. Dunn, J. A. O'Hara *et al.*, *J. Magn. Reson. Imaging* **16,** 511 (2002).
[g] T. Hasegawa, J. G. Rhee *et al.*, *Int. J. Radiat. Oncol. Biol. Phys.* **13,** 569 (1987).
[h] C. W. Song, A. Shakil *et al.*, *Int. J. Hyperthermia* **12,** 367 (1996).

[i] M. J. Eble, F. Wenz *et al.*, *in* "Tumor Oxygenation" (P. W. Vaupel, D. K. Kelleher, and M. Günderoth, eds.), p. 95. Gustav Fischer, Stuttgart, Germany, 1995.
[j] S. Falk, V. Laurence *et al.*, *in* "Tumor Oxygenation" (P. W. Vaupel, D. K. Kelleher, and M. Günderoth, eds.), p. 281. Gustav Fischer, Stuttgart, Germany, 1995.
[k] M. Höckel, K. Schlenger *et al.*, *Semin. Radiat. Oncol.* **6,** 3 (1996).
[l] D. W. Siemann, I. M. Johansen *et al.*, *Int. J. Radiat. Oncol. Biol. Phys.* **40,** 1171 (1998).
[m] D. F. Wilson, *in* "Oxygen Transport to Tissue XIV" (W. Erdmann and D. F. Bruley, eds.), p. 195. Plenum Press, New York, 1992.
[n] S. A. Vinogradov, L.-W. Lo *et al.*, *Biophys. J.* **70,** 1609 (1996).
[o] M. W. Dewhirst, E. T. Ong *et al.*, *Br. J. Cancer* **79,** 1717 (1999).
[p] K. Erickson, R. D. Braun *et al.*, *Cancer Res.* **63,** 4705 (2003).
[q] A. A. Potapov, E. B. Sirovskii *et al.*, *Vopre. Neirokhir.* **1,** 20 (1979).

Reporter molecules have been developed for use with electron spin resonance (ESR or EPR), where the line width is highly sensitive to oxygen.[28,44–55] Two primary approaches are used: (1) direct intratumoral (IT) injection of char crystals,[49,56] phthalocyanine,[57] or India ink[58] into a tissue or (2) intravenous (IV) infusion of water-soluble agents which disseminate throughout the tumor vasculature.[47,53] Direct IT injection is invasive and has generally been applied as a spectroscopic approach to report pO_2 at single locations only. Nonetheless, significant data have been achieved demonstrating hypoxiation and reoxygenation with respect to irradiation, and the importance of timing successive radiation doses to coincide with reoxygenation.[59] Char particles may be stable in tissue for weeks to years, allowing measurements of chronic changes in tissues (e.g., accompanying tumor growth).[28] The IV approach is noninvasive, but reporter molecules may predominately distribute in the well-perfused vasculature, potentially biasing measurements toward the well-oxygenated tumor regions. Progressive uptake and clearance of agents produces variable concentrations, and some agents degrade in tissue requiring appropriate correction factors.[47] Nonetheless, images of tumor oxygen distribution have been reported, including three-dimensional representations.[53] Spin radicals also may be applied to a combined ESR–NMR (nuclear magnetic resonance) approach, Overhauser-enhanced magnetic resonance imaging (OMRI), exploiting the Overhauser enhancement in the tissue water proton MRI signal that occurs by polarization transfer from free radicals upon electromagnetic irradiation.[60]

[44] H. M. Swartz, S. Boyer *et al.*, *Magn. Reson. Med.* **20,** 333 (1991).
[45] H. M. Swartz, S. Boyer *et al.*, *in* "Oxygen Transport to Tissue XIV" (W. Erdmann and D. F. Bruley, eds.), p. 221. Plenum Press, New York, 1992.
[46] H. M. Swartz, K. J. Liu *et al.*, *Magn. Reson. Med.* **31,** 229 (1994).
[47] P. Kuppusamy, R. Afeworki *et al.*, *Cancer Res.* **58,** 1562 (1998).
[48] B. F. Jordan, P. Misson *et al.*, *Int. J. Radiat. Oncol. Biol. Phys.* **48,** 565 (2000).
[49] J. He, N. Beghein *et al.*, *Magn. Reson. Med.* **46,** 610 (2001).
[50] H. Jiang, N. Beghei *et al.*, *Phys. Med. Biol.* **46,** 3323 (2001).
[51] P. E. James and H. M. Swartz, *Methods Enzymol.* **350,** 52 (2002).
[52] B. F. Jordan, V. Gregoire *et al.*, *Cancer Res.* **62,** 3555 (2002).
[53] M. Elas, B. B. Williams *et al.*, *Magn. Reson. Med.* **49,** 682 (2003).
[54] B. F. Jordan, N. Beghein *et al.*, *Int. J. Cancer* **103,** 138 (2003).
[55] P. Mahy, M. De Bast *et al.*, *Radiother. Oncol.* **67,** 53 (2003).
[56] N. Vahidi, R. B. Clarkson *et al.*, *Magn. Reson. Med.* **31,** 139 (1994).
[57] J. F. Glockner and H. M. Swartz, *in* "Oxygen Transport to Tissue XIV" (W. Erdmann and D. F. Bruley, eds.), p. 229. Plenum Press, New York, 1992.
[58] F. Goda, K. Jian Lu *et al.*, *Magn. Reson. Med.* **33,** 237 (1995).
[59] J. A. O'Hara, F. Goda *et al.*, *Radiat. Res.* **150,** 549 (1998).
[60] M. C. Krishna, S. English *et al.*, *Proc. Natl. Acad. Sci. USA* **99,** 2216 (2002).

Vascular oxygenation has been probed by fluorescence or phosphorescence imaging based on reporter complexes delivered IV.[61,62] Historically, the approach was limited to superficial tissues due to limited light penetration. The latest molecules are active in the near-infrared, permitting greater depth of signal penetration.[63]

NMR facilitates interrogation of deep tissues noninvasively, and ^{19}F NMR approaches will be reviewed in detail in the following section. The methods discussed earlier provide direct quantitative measurements of pO_2 based on various physiochemical parameters, such as electric current, fluorescent lifetime, magnetic resonance linewidth, or relaxation. Other approaches are less direct, but can reveal hypoxia or correlates of pO_2.

Specific classes of reporter molecules have been developed to reveal hypoxia[26,64] (e.g., pimonidazole,[65,66] EF5,[67,68] CCl-103F,[69] Cu-ATSM[70,71] galactopyranoside IAZA[72]). Following IV infusion, these agents become reduced in tissues and are trapped. However, in the presence of oxygen they are reoxidized and ultimately clear from the body. Histologic assessment of the distribution of these agents provides microscopic indications of local hypoxia. EF5, pimonidazole, and Cu-ATSM are currently being tested in clinical trials, and correlations have been reported with clinical outcome.[66,67,70] Many variants have been proposed over the past 20 years, and incorporation of radionuclides has facilitated noninvasive investigations using positron emission tomography (PET) or single photon emission computed tomography (SPECT), while ^{19}F labels permitted NMR spectroscopy.[72–74] Generally, only a single time point is investigated, but dynamic variations in hypoxia may be assessed, even in biopsy specimens, by applying pairs of hypoxia reporters in a pulse-chase fashion with respect to an intervention, as shown by Ljungkvist *et al.*[69]

[61] D. Wilson and G. Cerniglia, *Cancer Res.* **52,** 3988 (1992).
[62] G. Helminger, F. Yuan *et al.*, *Nature Med.* **3,** 177 (1997).
[63] D. F. Wilson, S. A. Vinogradov *et al.*, *Comp. Biochem. Physiol., Part A Mol. Integr. Physiol.* **132,** 153 (2002).
[64] J. R. Ballinger, *Semin. Nucl. Med.* **31,** 321 (2001).
[65] J. A. Raleigh, S. C. Chou *et al.*, *Radiat. Res.* **151,** 580 (1999).
[66] J. H. A. M. Kaanders, K. I. E. M. Wijffels *et al.*, *Cancer Res.* **62,** 7066 (2002).
[67] S. M. Evans, S. Hahn *et al.*, *Cancer Res.* **60,** 2018 (2000).
[68] W. R. Dolbier, Jr., A. R. Li *et al.*, *Appl. Radiat. Isotop.* **54,** 73 (2001).
[69] A. S. E. Ljungkvist, J. Bussink *et al.*, *Int. J. Radiat. Oncol. Biol. Phys.* **48,** 1529 (2000).
[70] F. Dehdashti, P. W. Grigsby *et al.*, *Int. J. Radiat. Oncol. Biol. Phys.* **55,** 1233 (2003).
[71] F. Dehdashti, M. A. Mintun *et al.*, *Eur. J. Nucl. Med. Molec. Imaging* **30,** 844 (2003).
[72] J. D. Chapman, E. L. Engelhardt *et al.*, *Radiother. Oncol.* **46,** 229 (1998).
[73] R. J. Maxwell, P. Workman *et al.*, *Int. J. Radiat. Oncol. Biol. Phys.* **16,** 925 (1989).
[74] R. J. Hodgkiss, *Anticancer Drug Des.* **13,** 687 (1998).

Several studies have shown a lack of correlation between hypoxic marker binding and pO_2 assessed using the Eppendorf Histograph, which may be related to chronic versus acute hypoxia, or the extent of necrosis.[75–77] The ultimate value of the techniques is evidenced by correlations between uptake and outcome.[66,70,71,78] Recent data also indicate that EF5 fluorescence may be correlated with pO_2.[79]

The techniques discussed so far all depend on exogenous reporter molecules or probes. Ideally, oxygenation could be related to endogenous characteristics. Because many biochemical pathways are under oxygen regulation, they can provide an elegant window on hypoxia, for example, induction of hypoxia-inducible factor 1 (HIF-1) and glucose transporter 1 (Glut-1) together with secondary responses, such as increased production of vascular endothelial growth factor (VEGF), NIP3 and tumor-associated macrophage activity.[8] Such molecules indicate hypoxia, though they may be induced by other factors. Intrinsic radiation sensitivity also may be assessed using the Comet assay.[80] These assays each require biopsy. Other markers potentially associated with hypoxia may be found in the plasma or urine and have been correlated with clinical outcome.[81] An attractive alternative is the introduction of transgenes with hypoxic response elements (HREs) as promoter sequences coupled to reporter genes such as GFP (green fluorescent protein)[82,83] or luciferase.[84,85] GFP synthesis is an energetic process, which could be hindered under hypoxia conditions. Likewise, bioluminescence accompanying action of luciferase on luciferin requires adenosine triphosphate (ATP) and O_2, but reports suggest that even under exceedingly low pO_2, sufficient oxygen remains to reveal hypoxia.

Many practical considerations govern clinical application of oximetry methods. Proton MRI is routinely applied for anatomic evaluation of tumors and would provide an ideal conduit for prognostic investigations. Application of contrast agents may reveal tumor boundaries to enhance detectability, and the dynamic contrast enhancement (DCE) changes provide insight into vascular perfusion and surface permeability area.[86]

[75] W. T. Jenkins, S. M. Evans *et al.*, *Int. J. Radiat. Oncol. Biol. Phys.* **46,** 1005 (2000).
[76] P. L. Olive, J. P. Banath *et al.*, *Acta Oncol.* **40,** 917 (2001).
[77] M. Nordsmark, J. Loncaster *et al.*, *Radiother. Oncol.* **67,** 35 (2003).
[78] C. J. Koch, S. M. Hahn *et al.*, *Cancer Chemother. Pharmacol.* **48,** 177 (2001).
[79] C. J. Koch, *Methods Enzymol.* **352,** 3 (2002).
[80] P. L. Olive, P. J. Johnston *et al.*, *Nature Med.* **4,** 103 (1998).
[81] Q. T. Le, P. D. Sutphin *et al.*, *Clin. Cancer Res.* **9,** 59 (2003).
[82] Y. Cao, C. Li *et al.*, "A Study of Hypoxia-Induced Gene Expression in Human Tumors." 48th Annual Meeting of Radiation Research, San Juan, Puerto Rico, 2001.
[83] D. Vordermark, T. Shibata *et al.*, *Neoplasia* **3,** 527 (2001).
[84] T. Shibata, A. J. Giaccia *et al.*, *Gene Ther.* **7,** 493 (2000).
[85] E. Payen, M. Bettan *et al.*, *J. Gene Med.* **3,** 498 (2001).
[86] A. R. Padhani, *J. Magn. Reson. Imaging* **16,** 407 (2002).

Specific studies have shown a correlation between DCE and pO_2,[87] and indeed, a theoretical underpinning has been provided based on the Krogh cylinder model.[88] However, the correlation is unlikely to be widely applicable, since DCE is sensitive to vascular flow, perfusion, and permeability, where pO_2 depends on oxygen consumption as well as delivery.

Blood oxygen level dependent (BOLD) contrast proton NMR facilitates rapid interrogation of vascular oxygenation and is particularly appropriate for examining dynamic responses to interventions.[48,89–91] Deoxyhemoglobin is paramagnetic and induces signal loss in T_2*-weighted images. However, BOLD does not provide absolute pO_2 values and is confounded by the influence of blood flow, as investigated extensively by Howe *et al.*,[92] who termed the expression *FLOOD* (flow and oxygen level dependent) contrast. In addition, variation in vascular volume can introduce signal perturbation.[93] Nonetheless, some studies have indicated a correlation with relative pO_2, but poor indication of absolute pO_2.[53,94,95]

Near-infrared spectroscopy (NIRS) offers an alternative approach based on the differential light absorption of the strong chromophores oxyhemoglobin and deoxyhemoglobin. NIRS provides a noninvasive means to monitor global tumor vascular oxygenation in real time based on endogenous molecules. Although many NIRS investigations have been conducted in the brain and breast in both laboratory and clinical settings over the past decade, there have been relatively few reports regarding solid tumors.[43,96–106] Most studies to date have used reflectance mode. By contrast, we have favored transmission mode, so as to interrogate deep tumor regions, and we have presented preliminary studies in rat breast

[87] R. A. Cooper, B. M. Carrington *et al.*, *Radiother. Oncol.* **57,** 53 (2000).
[88] Z. Wang, M.-Y. Su *et al.*, *Technol. Cancer Res. Treat.* **1,** 29 (2002).
[89] H. A. Al-Hallaq, J. N. River *et al.*, *Int. J. Radiat. Oncol. Biol. Phys.* **41,** 151 (1998).
[90] S. P. Robinson, F. A. Howe *et al.*, *Semin. Radiat. Oncol.* **8,** 198 (1998).
[91] R. Mazurchuk, R. Zhou *et al.*, *Magn. Reson. Imaging* **17,** 537 (1999).
[92] F. A. Howe, S. P. Robinson *et al.*, *Magn. Reson. Imaging* **17,** 1307 (1999).
[93] F. A. Howe, S. P. Robinson *et al.*, *NMR Biomed.* **14,** 497 (2001).
[94] C. Baudelet and G. Gallez, *Magn. Reson. Med.* **48,** 980 (2002).
[95] X. Fan, J. N. River *et al.*, *Int. J. Radiat. Oncol. Biol. Phys.* **54,** 1202 (2002).
[96] H. D. Sostman, S. Rockwell *et al.*, *Magn. Reson. Med.* **20,** 253 (1991).
[97] R. G. Steen, K. Kitagishi *et al.*, *J. Neurooncol.* **22,** 209 (1994).
[98] F. Steinberg, H. J. Rohrborn *et al.*, *Adv. Exp. Med. Biol.* **428,** 553 (1997).
[99] E. L. Hull, D. L. Conover *et al.*, *Br. J. Cancer* **79,** 1709 (1998).
[100] B. J. P. van der Sanden, A. Heerschap *et al.*, *Magn. Reson. Med.* **42,** 490 (1999).
[101] H. Liu, Y. Song *et al.*, *Appl. Op.* **39,** 5231 (2000).
[102] M. Kragh, B. Quistorff *et al.*, *Eur. J. Cancer* **37,** 924 (2001).
[103] G. Gulsen, H. Yu *et al.*, *Technol. Cancer Res. Treat.* **1,** 497 (2002).
[104] E. L. Heffer and S. Fantini, *Appl. Opt.* **41,** 3827 (2002).
[105] T. O. McBride, B. W. Pogue *et al.*, *J. Biomed. Opt.* **7,** 72 (2002).
[106] J. G. Kim, D. Zhao *et al.*, *J. Biomed. Optics* **8,** 53 (2003).

and prostate tumors with respect to various interventions.[43,101,106] NIR approaches are presented in detail in Chapter 17 of this volume.

Each technique has specific virtues and drawbacks, which must be considered for any given application, particularly the degree of invasiveness, the ability to generate maps of heterogeneity, and the ability to assess dynamic changes. In addition, the location of a measurement (e.g., vascular versus tissue compartments, the precision of measurements, and spatial and temporal resolution) must be considered. For further details of the techniques described earlier, the reader is referred to the references. In the next section, we present ^{19}F NMR approaches in greater detail.

^{19}F NMR Approaches to Measuring pO_2

Nuclear magnetic resonance (NMR) is attractive because it is inherently noninvasive. Liquid-state NMR is characterized by several parameters, including signal amplitude, chemical shift (δ), spin–spin relaxation (T_2), and spin–lattice relaxation (T_1). Oxygen could be quantified using ^{17}O NMR, but this is rather esoteric.[107] Alternatively, it has long been recognized that the oxygen molecule (O_2) is paramagnetic, causing increased spin–lattice relaxation rates ($R_1 = 1/T_1$). Indeed, physical and theoretical chemists must go to great lengths to rigorously remove oxygen from solutions (using freeze–thaw procedures) to achieve inherent relaxation rates for studying nuclear interactions.[108] Proton NMR studies have reported changes in the water relaxation rate as a result of tissue oxygenation,[109] but many other processes (metal ions, cellularity, pH, ionic strength) also cause relaxation, and thus it is not suitable for detecting pO_2, except under rare circumstances, such as with the eye.[110] There is also a substantial temperature response, whereas the relaxivity due to oxygen is only 0.0002 s^{-1}/torr.[110]

However, several investigators showed that the ^{19}F NMR spin–lattice relaxation rates for fluorocarbons are much more sensitive to pO_2.[111,112] Thomas *et al.*[113] pioneered the application of ^{19}F NMR relaxometry to measure pO_2 in tissues, *in vivo*, including lung, liver, and spleen; several other investigators demonstrated feasibility and applications,[114–120] as

[107] X. H. Zhu, H. Merkle *et al.*, *Magn. Reson. Med.* **45,** 543 (2001).
[108] M. A. Hamza, G. Serratice *et al.*, *J. Magn. Reson.* **42,** 227 (1981).
[109] E. Tadamura, H. Hatabu *et al.*, *J. Magn. Reson. Imaging* **7,** 220 (1997).
[110] B. A. Berkowitz, C. McDonald *et al.*, *Magn. Reson. Med.* **46,** 412 (2001).
[111] J.-J. Delpuech, M. A. Hamza *et al.*, *J. Chem. Phys.* **70,** 2680 (1979).
[112] M. A. Hamza, G. Serratice *et al.*, *J. Am. Chem. Soc.* **103,** 3733 (1981).
[113] S. R. Thomas, *in* "Magnetic Resonance Imaging" (C. L. Partain, R. R. Price, J. A. Patton, M. V. Kulkarni, and A. E. J. James, eds.), Vol. 2, p. 1536. W. B. Saunders, London, 1988.
[114] J. E. Fishman, P. M. Joseph *et al.*, *Magn. Reson. Imaging* **5,** 279 (1987).

reviewed some years ago by Mason.[121] The ^{19}F NMR R_1 of perfluorocarbons (PFCs) varies linearly with pO_2,[113,122] and each resonance is sensitive to pO_2, temperature, and magnetic field, but importantly, is essentially unresponsive to pH, CO_2, charged paramagnetic ions, mixing with blood, or emulsification.[123–127]

A particular PFC molecule may have multiple resonances, and each resonance has a characteristic R_1 response to pO_2. This is attributed to steric effects of O_2, as it approaches the molecule,[112] which implies that perfluorinated groups, which are both geometrically and magnetically comparable, should have similar R_1 responses to oxygen tension. At a fixed temperature and magnetic-field strength, the R_1 response to pO_2 of any single resonance obeys the simple formula

$$R_1 = R_{1a} + (R_{1p}X) \tag{1}$$

where X is the mole fraction of O_2 dissolved in the PFC, R_{1a} is the anoxic relaxation rate, and R_{1p} is the relaxation rate due to the paramagnetic contribution of oxygen. According to Henry's law, the dissolved mole fraction is related directly to the partial pressure of oxygen,

$$pO_2 = KX \tag{2}$$

where K represents Henry's constant for a given solution of gas at a specified temperature. By substitution,

$$R_1 = R_{1a} + (R_{1p}/K)pO_2 \tag{3}$$

The slope (R_{1p}/K) indicates the response of a particular resonance to pO_2.

PFCs essentially act as molecular amplifiers, since the solubility of oxygen is greater than in water, but thermodynamics require that the pO_2 in the PFC will rapidly equilibrate with the surrounding medium, and estimates of diffusion suggest the equilibration can occur within seconds.

[115] S. K. Holland, R. P. Kennan *et al.*, *Magn. Reson. Med.* **29,** 446 (1993).
[116] B. R. Barker, R. P. Mason *et al.*, *J. Magn. Reson. Imaging* **4,** 595 (1994).
[117] B. J. Dardzinski and C. H. Sotak, *Magn. Reson. Med.* **32,** 88 (1994).
[118] U. Noth, S. P. Morrissey *et al.*, *Magn. Reson. Med.* **34,** 738 (1995).
[119] H. T. Tran, Q. Guo *et al.*, *Acad. Radiol.* **2,** 756 (1995).
[120] S. Laukemper-Ostendorf, A. Scholz *et al.*, *Magn. Reson. Med.* **47,** 82 (2002).
[121] R. P. Mason, *Artif. Cells Blood Substit. Immobil. Biotechnol.* **22,** 1141 (1994).
[122] P. Parhami and B. N. Fung, *J. Phys. Chem.* **87,** 1928 (1983).
[123] L. C. Clark, Jr., J. Ackerman *et al.*, *in* "Oxygen Transport to Tissue VI" (D. Bruley, H. I. Bicher, and D. Reneau, eds.), p. 835. Plenum Press, New York,.
[124] C. F. Kong, G. M. Holloway *et al.*, *J. Phys. Chem.* **88,** 6308 (1984).
[125] C.-S. Lai, S. Stair *et al.*, *J. Magn. Reson.* **57,** 447 (1984).
[126] D. Eidelberg, G. Johnson *et al.*, *Magn. Reson. Med.* **6,** 344 (1988).
[127] S. R. Thomas, R. G. Pratt *et al.*, *Radiology* **18,** 159 (1991).

TABLE II *(continued)*

PFC	Sensitivity to pO_2[a]	Temp. sensitivity (torr/°)	Magnetic field B_0(T)	Application/ comments	References
PFTB	A = 0.684 B = 0.00305		4.7	Rabbit eye	Berkowitz, Wilson *et al.*[166]; Wilson, Berkowitz *et al.*[b]
PFTB	A = 0.9072 B = 0.004486		1.5	Human eye	Wilson, Berkowitz *et al.*[167]
PFTB	A = 0.8848 B = 0.1307	8.17	7	Mouse Meth-A tumor and heart	Mason, Shukla *et al.*[141]
Perfluorotripropylamine (FTPA)	A = 0.314 B = 0.002760^{-3}		1.9	Rat subcutaneous tumor	Fishman, Joseph *et al.*[c]
FTPA	A = 0.301 B = 0.00312		1.4	Rat spleen, lung, liver	Fishman, Joseph *et al.*[114]
FTPA	A = 0.4052 B = 0.0023		2.0	Rat liver, spleen	Holland, Kennan *et al.*[115]
FTPA			4.4	Cells	Taylor and Deutsch[d]
Bis-perfluoro-butylethylene (F-44E)	A = 0.3421 B = 0.11172		7.05	Rat, alginate capsules	Noth, Grohn *et al.*[164]
F-44E	A = 0.342 B = 0.1201		7.05	Rat spleen, liver, abdominal aorta, vena cava	Noth, Morrissey *et al.*[118]
F-44E	A = 0.2525 B = 0.16527	0.59	2.0	Mouse tumor	Hees and Sotak[153]
Perfluoroctyl-bromide (perflubron) (PFOB)	A = 0.517 B = 0.0038		9.4	Rat heart	Shukla, Mason *et al.*[e]
PFOB	A = 0.2677 B = 0.12259	1.26	4.7	Prostate tumor in rat	Antich *et al.*[162]

PFOB	A = 0.328 B = 0.12137	2.85	7	Phantom	Mason, Shukla *et al.*[142]
PFOB			2.0	Rat tumor	Sostman, Rockwell *et al.*[96]
PFOB	A = 0.085 B = 0.0033		1.5	Rabbit liver	Tran, Guo *et al.*[119]
PFOB			8.5	Pig liver, lung, spleen	Millard and McGoron[f]
PFOB			1.45	Rat lung, Mouse lung	Thomas, Clark, Jr. *et al.*[g]
PFOB			1.5	Pig lung	Laukemper-Ostendorf, Scholz *et al.*[120]
Perfluoro-2,2,2′,2′-tetramethyl-4,4′-bis(1,3-fioxolane) (PTBD)	A = 0.50104 B = 0.1672		2.0	Phantom	Sotak, Hees *et al.*[h]

Some original papers presented calibration curves in other forms (e.g., including coefficients for temperature dependence). In those cases, equations have been derived assuming 37°. Where a PFC has more than one resonance, the equation presented is either for the most sensitive signal, or the equation used where the signal may have been unresolved.

[a] $R_1\ (s^{-1}) = A + B \times pO_2$ (torr).

[b] C. A. Wilson, B. A. Berkowitz *et al.*, *Exp. Eye Res.* **55,** 119 (1992).

[c] J. E. Fishman, P. M. Joseph *et al.*, *Invest. Radiol.* **24,** 65 (1989).

[d] J. Taylor and C. J. Deutsch, *Biophys. J.* **53,** 227 (1988).

[e] H. P. Shukla, R. P. Mason *et al.*, *Magn. Reson. Med.* **35,** 827 (1996).

[f] R. W. Millard and A. J. McGoron, *Artif. Cells Blood Subst. Immobil. Biotechnol.* **22,** 1251 (1994).

[g] S. R. Thomas, L. C. Clark, Jr. *et al.*, *J. Comput. Assist. Tomogr.* **10,** 1 (1986).

[h] C. H. Sotak, P. S. Hees *et al.*, *Magn. Reson. Med.* **29,** 188 (1993).

Because relaxation is proportional to oxygen concentration, the effect will be greater at a given pO_2 than for water. Importantly, ions do not enter the hydrophobic PFC phase, and thus do not affect the bulk relaxation. Indeed, PFCs are typically exceedingly hydrophobic and do not mix with the aqueous phases, but rather form droplets or emulsions. Based on these principles, PFCs have been applied to *in vivo* pO_2 measurements. Characteristics of many diverse PFCs are summarized in Table II.

At any given magnetic field (Bo) and temperature (T), sensitivity to changes in pO_2 is given by $R_1 = a + bpO_2$. Thus a greater slope is important, and the ratio $\eta = b/a$ has been proposed as a sensitivity index.[128] Generally, a small "a" value (intercept) represents greater sensitivity, but it also generates longer T_1 values under hypoxic conditions, potentially increasing data acquisition times. Indeed, the T_1 of hexafluorobenzene (HFB) at 4.7 T may reach 12 s, potentially creating long imaging cycles, but this is readily overcome by applying single-shot (echo planar) imaging techniques, as presented in a later section.

Many PFCs, such as perfluorotributylamine (PFTB), perflubron (formerly referred to as perfluorooctyl bromide; PFOB), and Therox (F44-E), have several ^{19}F NMR resonances, which can be exploited to provide additional information in spectroscopic studies, but seriously hamper effective imaging. Multiple resonances can lead to chemical shift artifacts in images, which compromise the integrity of relaxation time measurements, though they can be avoided by selective excitation, or detection, chemical shift imaging, deconvolution, or sophisticated tricks of NMR spin physics.[116,119,129–133] These approaches add to experimental complexity and are generally associated with lost signal to noise ratio (SNR). Thus we strongly favor PFCs with a single resonance, and we will describe the use of HFB,[27,32,42,106,134–137] though some research groups favor 5-crown-5-ether (15C5).[88,117,138,139]

[128] S. R. Thomas, R. G. Pratt *et al.*, *Magn. Reson. Imaging* **14,** 103 (1996).
[129] L. J. Busse, R. G. Pratt *et al.*, *J. Comp. Ast. Tomagr.* **12,** 824 (1988).
[130] R. P. Mason, N. Bansal *et al.*, *Magn. Reson. Imaging* **8,** 729 (1990).
[131] H. K. Lee and O. Nalcioglu, *J. Magn. Reson. Imaging* **2,** 53 (1992).
[132] U. Nöth, R. Deichmann *et al.*, *J. Magn. Reson. B* **105,** 233 (1994).
[133] R. G. Pratt, J. Zheng *et al.*, *Magn. Reson. Med.* **37,** 307 (1997).
[134] D. Zhao, A. Constantinescu *et al.*, *Radiat. Res.* **156,** 510 (2001).
[135] Y. Song, A. Constantinescu *et al.*, *Technol. Cancer Res. Treat.* **1,** 471 (2002).
[136] D. Zhao, A. Constantinescu *et al.*, *Radiat. Res.* **159,** 621 (2003).
[137] D. Zhao, S. Ran *et al.*, *Neoplasia* **5,** 308 (2003).
[138] B. P. J. van der Sanden, A. Heerschap *et al.*, *Int. J. Radiat. Oncol. Biol. Phys.* **44,** 649 (1999).
[139] T. Q. Duong, C. Ladecola *et al.*, *Magn. Reson. Med.* **45,** 61 (2001).

TABLE II
^{19}F NMR CHARACTERISTICS AND APPLICATIONS OF PFCs FOR TISSUE OXIMETRY

PFC	Sensitivity to pO_2[a]	Temp. sensitivity (torr/°)	Magnetic field B_0(T)	Application/ comments	References
Hexafluorobenzene (HFB)	A = 0.0835 B = 0.001876	0.13	4.7	Rat breast tumor, prostate tumor, human lymphoma xenograft	Hunjan, Zhao *et al.*[159] Zhao, Constantinescu *et al.*[32,134,136]; Mason, Ran *et al.*[27]; Song, Constantinescu *et al.*[135]; Zhao, Ran *et al.*[137]
HFB	A = 0.074 B = 0.00158		4.7	Rat prostate tumor	Hunjan, Mason *et al.*[161]; Mason, Constantinescu *et al.*[175]
HFB	A = 0.093 B = 0.103	1.40	7	Phantom	Mason, Rodbumrung *et al.*[143]
Perfluoro-15-Crown-5-ether (15C5)	A = 0.345 B = 0.0034	2.94	2.0	Tumor cells	Helmer, Han *et al.*[157]
15C5	A = 0.333 B = 0.0033	3.98	2.0	Mouse tumor, spleen, liver	Dardzinski and Sotak[117]
15C5	A = 0.44 B = 0.0028		4.3	Human glioma tumor in mice	van der Sanden, Heerschap *et al.*[100]; van der Sanden, Heerschap *et al.*[138]
15C5	A = 0.375 B = 0.00198		4.7	Rat breast tumor	Fan, River *et al.*[95]
15C5	A = 0.362 B = 0.1239		4.7	Rat brain	Duong, Ladecola *et al.*[139]
Perfluorotributyl-amine (FC-43) PFTB	A = 1.09 B = 0.00623	4.43	0.14	Pig liver, spleen, lung	Thomas, Pratt *et al.*[128]
PFTB			0.14	Rat liver, spleen, lung	Pratt, Zheng *et al.*[133]; Thomas, Gradon *et al.*[163]

(continued)

R_1 is sensitive to temperature, although the response varies greatly between PFCs and between individual resonances of each individual PFC. Over small temperature ranges, a linear correction to calibration curves is appropriate, but over larger temperature ranges, the response can be complex, as investigated extensively by Shukla *et al.*[140] for several PFCs. Differential sensitivity of pairs of resonances to pO_2 and temperature allowed Mason *et al.*[141] to simultaneously determine both parameters by solving simultaneous equations. However, generally it is preferable for a pO_2 sensor to exhibit minimal response to temperature, since this is not always known precisely *in vivo* and temperature gradients may occur across tumors. As shown in Table II, even a relatively small error in temperature estimate can introduce a sizable discrepancy into the apparent pO_2; for example, the relative error introduced into a pO_2 determination by a 1° error in temperature estimate ranges from 8 torr/° for PFTB[141] to 3 torr/° for PFOB (perflubron)[142] or 15C5[117] and 0.1 torr/° for HFB,[143] when pO_2 is actually 5 torr. It must be noted that error depends on actual pO_2 and the error varies with magnetic field and temperature. R_1 response does depend on magnetic field, necessitating calibration curves for each type of magnet system (e.g., 1.5, 4.7, or 7 T). Thus comparison of PFC utility for pO_2 measurements is complicated by the field used for specific published investigations, and in Table II, we consider sensitivity as presented.

Choice of PFC may be governed by practical considerations, such as cost and availability, since several products, particularly proprietary emulsions, may be difficult to obtain. HFB and 15C5 offer the immediate advantage of a high symmetry and a single ^{19}F NMR resonance. This offers maximum SNR and simplifies imaging, which may otherwise require frequency selective excitation, deconvolution, or other NMR tricks to avoid chemical shift artifacts.

Route of Administration. The most popular route for the delivery of PFCs is as emulsions injected intravenously. Given the extremely hydrophobic nature of PFCs, they do not dissolve in blood directly, but may be formulated as biocompatible emulsions. Much effort has been applied to formulate stable homogenous emulsions, as reviewed elsewhere.[144] Following IV infusion, the emulsion circulates in the vasculature with a

[140] H. P. Shukla, R. P. Mason *et al.*, *J. Magn. Reson. B* **106,** 131 (1995).
[141] R. P. Mason, H. P. Shukla *et al.*, *Magn. Reson. Med.* **29,** 296 (1993).
[142] R. P. Mason, H. P. Shukla *et al.*, *Biomater. Artif. Cells Immobilization Biotechnol.* **20,** 929 (1992).
[143] R. P. Mason, W. Rodbumrung *et al.*, *NMR Biomed.* **9,** 125 (1996).
[144] J. G. Riess, *Biomater. Artif. Cells Immobilization Biotechnol.* **20,** 183 (1992).

typical half-life of 12 h, (depending on the nature of the emulsion) providing substantial clearance within 2 days.[145,146] Primary clearance is by macrophage activity, leading to extensive accumulation in the liver, spleen, and bone marrow.[113,147] Indeed, this is a major shortcoming of IV delivery, since animals may exhibit extensive hepatomegaly or splenomegaly.[148] The emulsions are not toxic, and other than causing swelling, appear not to cause health problems. PFC clearance occurs from the liver with a typical half-life of 60 days for perfluorotripropylamine and 3 days for perflubron, with primary clearance by migration to the lungs and exhalation.[149]

Some investigators have examined pO_2 of tissues, while PFC remained in the blood, providing a vascular pO_2.[114,118,150] Flow can generate artifacts, and correction algorithms have been proposed.[151] Many investigators have measured pO_2 in liver, spleen, and tumors following clearance from the blood, thus providing measurement of tissue pO_2.[95,100,115,117–119,152–157]

Both spectroscopic and imaging approaches have been applied to tissue pO_2 measurements depending on the available SNR. It appears that uptake and distribution efficiency vary with tumor type, but in general, maximum signal is detected from the tumor periphery corresponding with regions of greater perfusion.[100,117,138,154,158,159] Several reports have examined changes in tumor pO_2 in response to acute interventions such as vasoactive drugs and hyperoxic gases.[32,95,100,135–137,153,160] Spectroscopic time resolution has ranged from seconds to minutes,[161,162] whereas imaging often takes longer.[160]

Long tissue retention facilitates chronic studies during tumor development, and progressive tumor hypoxiation has been observed over extended time periods of many days.[154,156] Correlated ^{19}F and proton MRI suggest

[145] M. C. Malet-Martino, D. Betbeder *et al.*, *J. Pharm. Pharmacol.* **36,** 556 (1984).
[146] T. F. Zuck and J. G. Riess, *Crit. Rev. Clin. Lab. Sci.* **31,** 295 (1994).
[147] R. P. Mason, P. P. Antich *et al.*, *Magn. Reson. Imaging* **7,** 475 (1989).
[148] W. I. Rosenblum, M. G. Hadfield *et al.*, *Arch. Pathol. Lab. Med.* **100,** 213 (1976).
[149] R. F. Mattrey and D. C. Long, *Invest. Radiol.* **23,** s298 (1988).
[150] D. Eidelberg, G. Johnson *et al.*, *J. Cereb. Blood Flow P. Metab.* **8,** 276 (1988).
[151] T. Higuchi, S. Naruse *et al.*, *in* "7th SMRM," p. 435, 1988.
[152] R. P. Mason, R. L. Nunnally *et al.*, *Magn. Reson. Med.* **18,** 71 (1991).
[153] P. S. Hees and C. H. Sotak, *Magn. Reson. Med.* **29,** 303 and erratum **29,** 716 (1993).
[154] R. P. Mason, P. P. Antich *et al.*, *Int. J. Radiat. Oncol. Biol. Phys.* **29,** 95 (1994).
[155] S. R. Thomas, R. W. Millard *et al.*, *Artif. Cells Blood Subst. Immobil. Biotechnol.* **22,** 1029 (1994).
[156] N. J. Baldwin and T. C. Ng, *Magn. Reson. Imaging* **14,** 541 (1996).
[157] K. G. Helmer, S. Han *et al.*, *NMR Biomed.* **11,** 120 (1998).
[158] P. P. Antich, R. P. Mason, A. Constantinescu *et al.*, *Proc. Soc. Nucl. Med.* **35,** 216P (1994).
[159] D. J. O. McIntyre, C. L. McCoy *et al.*, *Curr. Sci.* **76,** 753 (1999).
[160] S. Hunjan, D. Zhao *et al.*, *Int. J. Radiat. Oncol. Biol. Phys.* **49,** 1097 (2001).
[161] R. P. Mason, F. M. H. Jeffrey *et al.*, *Magn. Reson. Med.* **27,** 310 (1992).
[162] S. Hunjan, R. P. Mason *et al.*, *Int. J. Radiat. Oncol. Biol. Phys.* **40,** 161 (1998).

that PFC does not redistribute, but remains associated with specific tissues, analogous to tree rings.[154,156] Thus in principle, a whole tumor can be investigated by administering successive doses of PFC emulsion during growth.

PFC emulsions may also be administered intraperitoneally (IP), resulting in similar distribution to IV administration (unpublished observations). Given the volatile nature of many PFCs, they could be inhaled, but although this is a popular route for delivery of anesthetics and blood flow tracers, it does not appear to have been widely exploited for oximetry. Nonetheless, aerosols have been delivered to the lungs by inhalation to facilitate pO_2 measurements.[163]

Two approaches have been applied to circumvent reticuloendothelial uptake. PFC has been incorporated in polyalginate beads for direct implantation at a site of interest.[164,165] We favor direct IT injection of neat PFC, allowing any region of interest in a tumor to be interrogated immediately. Use of a fine needle ensures minimal tissue damage, as described in detail in a later section. Others have used direct injection of emulsions into tumors, but this increases the volume considerably, making it more invasive.[88] Investigators have suggested that emulsification improves retention at the site of injection. Direct injection of neat PFC also has been used to investigate retinal oxygenation[166–168] and cerebral oxygenation in the interstitial and ventricular spaces.[139]

As described in the following section we favor direct intratumoral injection of neat HFB followed by echo planar imaging to generate pO_2 maps in tumors.

FREDOM (Fluorocarbon Relaxometry using Echo Planar Imaging for Dynamic Oxygen Mapping)

Recognizing that tumors are heterogeneous and that pO_2 may fluctuate, we developed a procedure, which allows repeated quantitative maps of regional pO_2 to be achieved with multiple individual locations simultaneously in 6.5 min with a precision of 1–3 torr, when pO_2 is in the

[163] S. R. Thomas, L. Gradon *et al.*, *Invest. Radiol.* **32,** 29 (1997).
[164] U. Nöth, P. Grohn *et al.*, *Magn. Reson. Med.* **42,** 1039 (1999).
[165] U. Zimmermann, U. Noth *et al.*, *Artif. Cells Blood Subst. Immobil. Biotechnol.* **28,** 129 (2000).
[166] B. A. Berkowitz, C. A. Wilson *et al.*, *Invest. Ophthalmol. Vis. Sci.* **32,** 2382 (1991).
[167] C. Wilson, B. Berkowitz *et al.*, *Arch. Ophthalmol.* **110,** 1098 (1992).
[168] W. Zhang, Y. Ito *et al.*, *Invest. Ophthalmol. Visual Sci.* **44,** 3119 (2003).

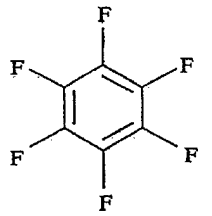

FIG. 1. Hexafluorobenzene (HFB) is a perfluorocarbon (PFC) exhibiting extensive symmetry.

range 0–10 torr.[160] We have applied FREDOM to diverse tumor types and interventions, as reviewed in a later section.

MRI is attractive because it is readily available at many institutions. For small animal work, ^{19}F NMR is widely available at 4.7, 7, and 9.4 T by minor adaptation of routine instrumentation, [e.g., retuning proton radiofrequency (RF) coils]. Within the recent past ^{19}F MRI is also becoming available on clinical systems, facilitating translation of these techniques to patients. ^{19}F NMR is particularly facile because there is essentially no background signal in tissues to interfere with measurements, yet the resonance frequency and sensitivity approach that of proton NMR. The pioneering work of Thomas[113] showed that tissue pO_2 could be imaged in various organs based on the ^{19}F NMR spin–lattice relaxation rate (R_1) of PFC reporter molecules following IV infusion. Prompted by these studies, we surveyed a number of PFCs and identified that HFB (Fig. 1) has many virtues as a pO_2 reporter.[143] Symmetry provides a single narrow ^{19}F NMR signal, and the spin–lattice relaxation rate is highly sensitive to changes in pO_2, yet minimally responsive to temperature (Fig. 2).[143] HFB also has a long spin–spin relaxation time (T_2), which is particularly important for imaging investigations. From a practical perspective, HFB is cheap (<$2/g) and readily available commercially in high purity (≥99%). We obtain supplies from Lancaster Synthesis (Windham, NH), though many other fine chemical supply houses also offer HFB. We do favor bottles over sealed ampoules, since they are easier to handle. HFB is well characterized in terms of lack of toxicity,[169,170] exhibiting no mutagenicity,[171] teratogenicity, or fetotoxicity,[172] and the manufacturer's material

[169] Y. S. Gorsman and T. A. Kapitonenko, *Izv. Estestvennonauchu. Inst. Pevinsk.* **15,** 155 (1973).
[170] I. M. C. M. Rietjens, A. Steensma *et al.*, *Eur. J. Pharmacol.* **293,** 292 (1995).
[171] K. E. Mortelmans and V. F. Simmon, *Gov. Rep. Announce. Index (US)* **81,** 2555 (1981).
[172] K. D. Courtney and J. E. Andrews, *J. Environ. Sci. Health B* **19,** 83 (1984).

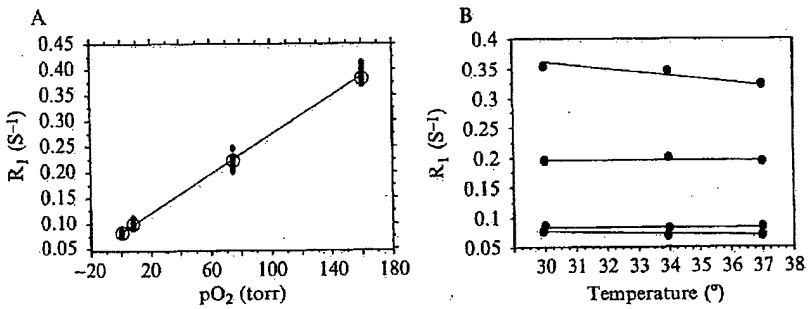

FIG. 2. (A) The ^{19}F NMR spin–lattice relaxation rate (R_1) of HFB shows a linear response to pO_2: at 37° and 4.7 T, $R_1 = 0.0835 + 0.001876 \times pO_2$. (B) The ^{19}F NMR R_1 of HFB shows minimal response to temperature in the physiologic range; separate curves are shown at four different pO_2s: 0, 1, 9.8, and 21% O_2.

data safety sheet indicates $LD_{50} > 25$ g/kg (oral—rat) and LC_{50} 95 g/m^3/2 h (inhalation—mouse).

HFB had been proposed as a veterinary anesthetic and has been used in many species, including ponies, sheep, cats, dogs, rats, and mice, but was abandoned because of its high volatility (boiling point 81°) and low flash point (10°).[173] This presented unacceptable dangers in veterinary suites for inhalation anesthetics. It is not a problem in our studies, where small quantities of liquid (typically, 50 μl) are injected directly into the tumor. HFB requires no special storage, other than a sealed bottle to prevent evaporation. Melting point is 4–6°, and density is 1.62 g/ml.

Methodology

Tumor Preparation. We have applied this technique to tumors in rats and mice, but our methodology will focus on our standard application to rats. As for electrode techniques, the tumor must be accessible (e.g., subcutaneous in flank of thigh), though we favor the pedicle model, which provides a tumor remote from the body, analogous to an additional limb.[174] This model is optimal for selective therapy such as local hyperthermia, irradiation, or excision. Noting the increasing interest in orthotopic tumors, the approach is also facile in breast tumors in the mammary fat pad and applicable in the prostate with a little practice.

[173] L. W. Hall, S. R. K. Jackson *et al.*, *in* "Recent Progress in Anaesthesiology and Resuscitation" (A. Arias, R. Llaurado, M. A. Nalda, and J. N. Lunn, eds.), p. 201. Excerpta Medica, Oxford, UK, 1975.

[174] E. W. Hahn, P. Peschke *et al.*, *Magn. Reson. Imaging* **11,** 1007 (1993).

Rats are preanesthetized with ketamine hydrochloride (100 mg/ml) as a relaxant and maintained under general gaseous anesthesia with air (1 dm^3/min) and 1.2% isoflurane [we do note that the appropriate concentration of anesthesia may depend on strain; for example, Copenhagen rats require (and tolerate) higher concentrations than Fisher rats]. In our latest refinement of the procedure, isoflurane may be stopped for a period of minutes during HFB administration, since rats occasionally exhibit respiratory distress, which may be caused by the anesthetic properties of HFB interacting with isoflurane. Within a few minutes, rats are stable and routine isoflurane anesthesia is maintained. In our earlier work we used 0.5% methoxyflurane in 33% oxygen with 66% N_2O,[160,175] but isoflurane appears to be a less stressful anesthetic.

HFB is deoxygenated by bubbling nitrogen for 5 min before use. We have previously shown in hypoxic tumor biopsies that use of aerated HFB may introduce a systematic apparent elevation in pO_2 (~2–3 torr). HFB is injected directly into tumors using a gas tight syringe with a custom-made fine sharp needle (32G #7803–04; Hamilton, Reno, NV). Generally, HFB is administered along three to five tracks in the form of a fan in a single central plane of the tumor coronal to the rat's body (Fig. 3A). The needle is inserted manually to penetrate across the whole tumor and withdrawn ~1 mm to reduce pressure, and 3 μl HFB is deposited. The needle is repeatedly withdrawn a further 2–3 mm, and additional HFB is deposited. Typically, HFB is deliberately deposited at about 16 individual locations per tumor, in both the central and peripheral regions of the tumors, to ensure that the interrogated regions are representative of the whole tumor.

The animal is placed on its side in a cradle with a thermal blanket to maintain body temperature. A fiber-optic probe is inserted rectally to monitor core temperature. Temperature measurement is optional, since the R_1 is essentially invariant with temperature and does not need correction for pO_2 estimates. Of course, temperature regulation and measurement is important to ensure stable tumor physiology. An MR-compatible pulse oximeter equipped with "rat" software (8600V; Nonin, Inc., Plymouth, MN) may be applied to a hind foot to monitor arterial oxygenation (S_aO_2) and heart rate (optional, but provides additional useful data regarding animal health and physiology).

Most of our MR experiments were performed using an Omega CSI 4.7 horizontal bore magnet system with actively shielded gradients (GE systems, acquired by Bruker Instrument, Inc., Fremont, CA). Recently, our MR system has been upgraded to a Varian Unity INOVA, providing

[175] R. P. Mason, A. Constantinescu *et al.*, *Radiat. Res.* **152,** 239 (1999).

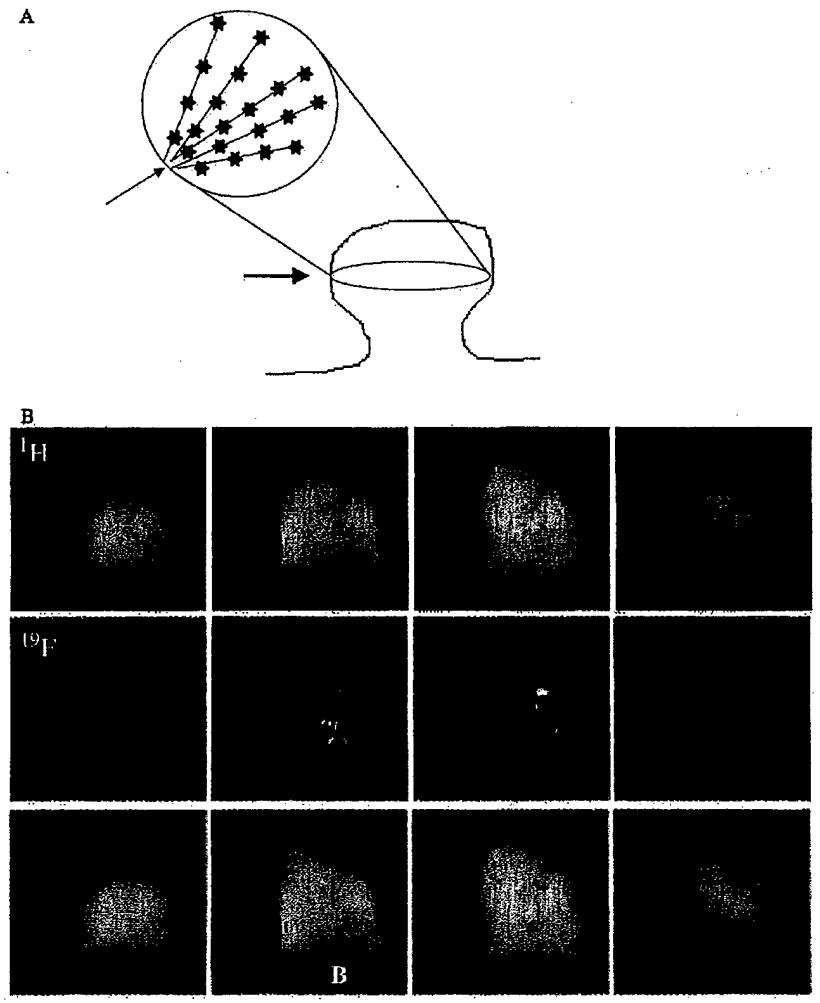

FIG. 3. (A) Recommended pattern of IT injection. Several tracks in the form of a fan in a single plane. (B) Four contiguous MR images (5 mm thick) of a representative Dunning prostate R3327-AT1 tumor (volume = 1.6 cm^3). *Top:* ^{1}H MRI; *middle:* corresponding ^{19}F; *bottom:* overlay to show interrogated regions. *B* marks point of attachment of the tumor to back of rat. (See color insert.)

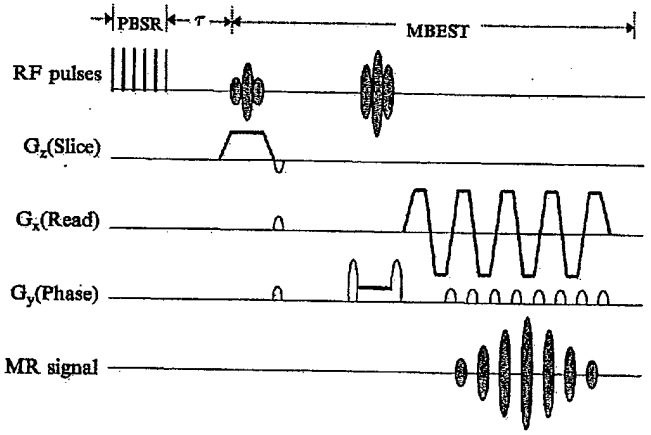

FIG. 4. MRI sequence used to achieve relaxation curves.

enhanced data acquisition and processing software and stronger imaging gradients. A tunable (^{1}H/^{19}F) MR coil, 2 or 3 cm in diameter matched to the tumor size (constructed from a cylindrical copper tube about 2 cm deep and acting as a single-turn solenoid), is placed around the tumor-bearing pedicle. Shimming is performed on the proton water signal to a typical linewidth of 60–100 Hz. Proton images are obtained for anatomic reference using a three-dimensional (3D) spin–echo sequence. The coil is then retuned in place to 188.27 MHz, and corresponding ^{19}F MR images are obtained. Overlaying the ^{19}F MR images on the corresponding proton images reveals the distribution of HFB (Fig. 3B). Typically, ^{19}F NMR signal is obtained from 6–10% of the total tumor voxels.[136,137,175]

pO_2 maps are obtained using our standard MR oximetry protocol.[116,160,176] This applies pulse burst saturation recovery (PBSR) echo planar imaging (EPI) relaxometry using the ARDVARC (*a*lternated *r*elaxation *d*elays with *v*ariable *a*cquisitions to *r*educe *c*learance effects) acquisition protocol to map the tumors (Fig. 4).[175,177] EPI uses a single spin–echo with "blipped" phase encoding (modulus-blipped echo-planar single-pulse technique [MBEST]), although other EPI sequences should be equally applicable. We chose the PBSR approach to T_1 relaxation measurements for historical reasons; our earliest work used ^{19}F NMR spectroscopy of tumors with excitation and detection based on surface coils.[152] The PBSR approach is suitable for use with the nonuniform excitation typical of surface

[176] B. R. Barker, R. P. Mason *et al.*, *Magn. Reson. Imaging* **11,** 1165 (1993).
[177] D. Le, R. P. Mason *et al.*, *Magn. Reson. Imaging* **15,** 971 (1997).

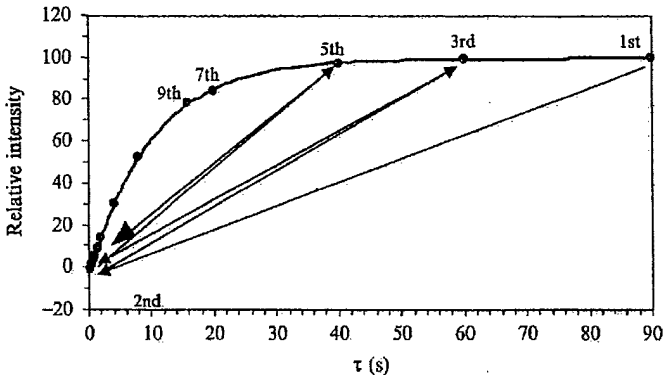

FIG. 5. Typical relaxation curve showing order of data acquisition. $y = A\,[1 - (1 + W)\exp(-R_1 \times \tau)]$ and $T_1 = 10.34 \pm 0.16$ s, A = 99.5, W = 0.04, and hence $pO_2 = 7.0 \pm 0.7$ torr.

coils as presented by Evelhoch and Ackerman.[178] For EPI, we do apply carefully calibrated $\pi/2$ pulses to ensure accurate refocusing of images, but we continue to favor the PBSR approach, since it provides particularly rapid estimation of T_1 by avoiding the need for extended relaxation recovery times between acquisitions. Saturation is achieved by a series of 20 nonspatially selective $\pi/2$ pulses with 50-ms spacing, which is sometimes called a "Comb" format.

Typical FREDOM parameters use 32 × 32 data points across a field of view of 40 × 40 mm, providing 1.25 mm in-plane resolution. Recently, we have applied a slice selection gradient, providing 5-mm-thick slices, and hence, 8-μl voxels. However, the deposition of HFB is designed to occur in a plane, and thus the discrete distribution of the reporter molecule itself can be used to define the slice. We apply a PBSR preparation sequence because it is ideally suited for measuring diverse, long T_1 values. Unlike more traditional inversion recovery sequences, there is no need to wait >5 T_1 between successive images. As shown in Fig. 5, we use 14 delays in the order 90 s, 200 ms, 60 s, 400 ms, 40 s, 600 ms, 20 s, 800 ms, 16 s, 1 s, 8 s, 1.5 s, 4 s, and 2 s, selected to cover the whole range of T_1s (viz pO_2 values). Many papers have been published on optimizing relaxation curves and choosing parameters to enhance precision.[179–181] Our experience suggests that our

[178] J. L. Evelhoch and J. J. H. Ackerman, *J. Magn. Reson.* **53,** 52 (1983).
[179] A. P. Crawley and R. M. Henkelman, *Magn. Reson. Med.* **7,** 23 (1988).
[180] S. J. Doran, J. J. Attard *et al.*, *J. Magn. Reson.* **100,** 101 (1992).
[181] F. Franconi, F. Seguin *et al.*, *Medical Phys.* **22,** 1763 (1995).

parameters are appropriate for interrogating a broad range of pO_2 values, though they have not been rigorously or theoretically optimized. More delays could improve curve fitting, but would increase experiment time. We believe fewer delays would degrade quality of the curve fitting.

Traditional T_1 measurement sequences acquire data with delays in monotonic order, whereas we alternate longer and shorter delays to minimize any systematic errors, which would be introduced if the signal amplitude varies during the measurement. We have found that HFB clears from tissue with a typical half-life of 600 min,[162] which would introduce errors into the amplitude. Although the total acquisition time for a T_1 map is 6.5 min, we reduce the time between first and last acquisitions further by applying the longest delay first. Our experience shows that it is important to measure at least two data points on the plateau of the curve (i.e., >5 × T_1, and we choose 60 and 90 s, respectively. The data points with longer recovery times have greater SNR, and we find that a minimum SNR = 10 is required to produce satisfactory T_1 curves and pO_2 estimates. The variation in amplitude between longest and shortest delays approaches 100-fold. The poorest SNR data points (short delay; τ) could compromise the quality of the T_1 curves, and thus we obtain multiple acquisitions at these times to provide enhanced SNR by signal averaging. Because the τ values are short, it adds little to the overall experimental time. We use NA = 12 for $\tau < 1$ s; NA = 8 for $\tau = 1$ s; NA = 4 for $\tau = 1.5$, 2, and 4 s; NA = 2 for $\tau = 8$ s; and 16 s and NA = 1 for the longer delays. Signal amplitudes are corrected for the additional acquisitions, and a 2-d Fourier transform (FT) is applied to each image. Curve fitting is then applied on a voxel-by-voxel basis to each image set. Data quality could probably be enhanced by application of apodization and filtering functions, such as Fermi and Hanning filters, though we have not yet implemented these approaches. The acquisition protocol is not part of the standard software supplied by the manufacturer, but we can assist interested investigators.

Data are transferred to a personal computer (PC) for further analysis using a program created in our laboratory (T_1map [Fig. 6], PASCAL by Dennis Le). T_1map recognizes issues in data analysis and provides filters, clustering algorithms, and temporospatial correlation to assist in effective data reduction. At top right of Fig. 6 is a map, which may be toggled to display signal amplitude, T_1, T_1 error ($T_{1\,err}$), or pO_2 (Fig. 7). Blank pixels indicate that no curve fit could be achieved. Gray pixels indicate a successful curve fit and potential pO_2 value, but with errors beyond the specified range. In this example, thresholds were set as $T_{1\,err} < 2.5$ s and the ratio $T_{1\,err}/T_1 < 50\%$. Tightening these thresholds can produce higher-quality data, but eliminates more data. Colored pixels report measurements satisfying the threshold criteria, and these are tabulated in the form of a

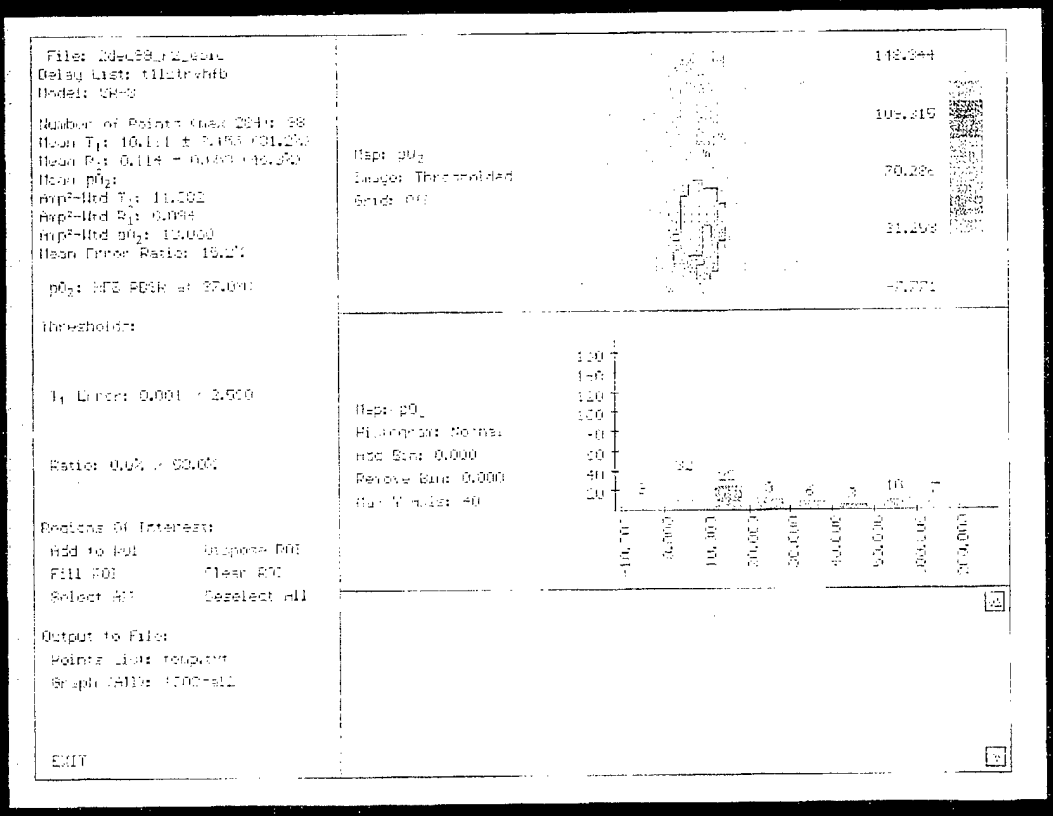

FIG. 6. Example T_1map used for data filtering, clustering, and analysis. (See color insert.)

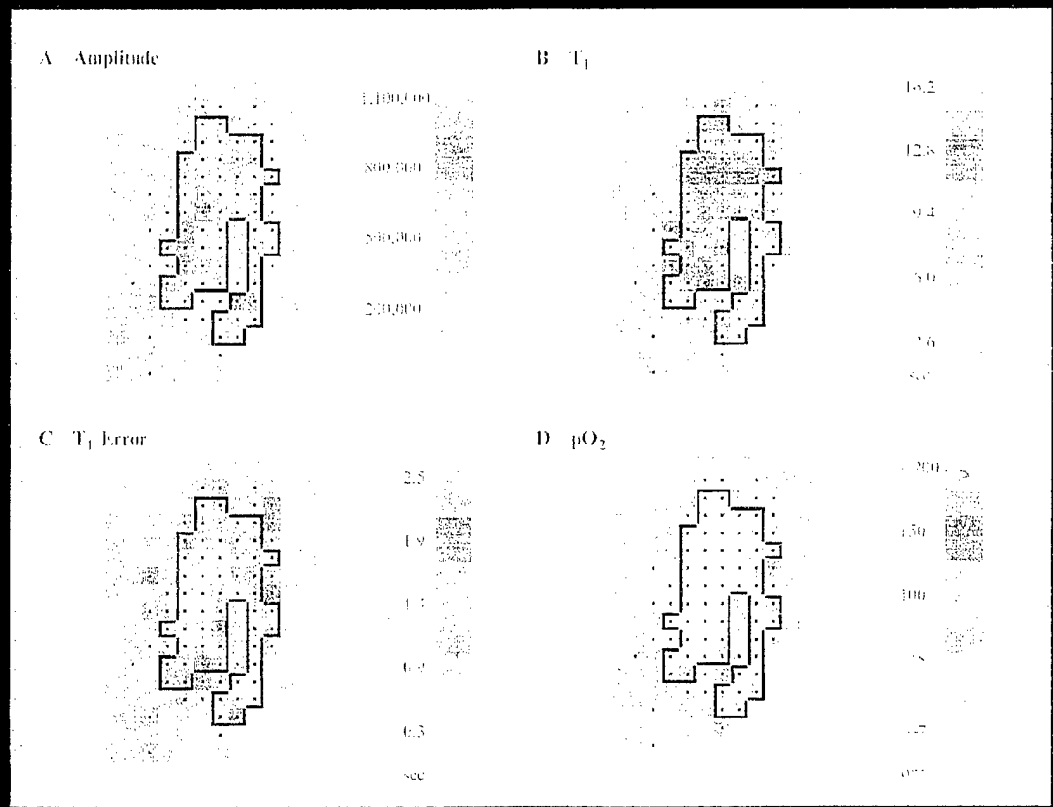

FIG. 7. *(continued)*

histogram (center), which can be plotted with selected data bins and ranges of interest. At bottom right of Fig. 6 are data for each pixel, including coordinate and fitted parameters. In the box on the left are shown the number of fitted data points, number of accepted data points, and statistics such as mean T_1, pO_2, and corresponding amplitude-weighted values.

pO_2 is calculated on the basis of a curve fit to exponential data. Any curve fitting is associated with uncertainty, and indeed our procedure determines $T_{1\,err}$ values. Although the concept of negative pO_2 values may appear impossible, it is perfectly reasonable, provided that error bars and uncertainties are considered. Thus a value of -2 torr $\pm$ 3 torr legitimately indicates an actual pO_2 very close to zero. Some oximetry approaches ignore negative values or bin them all as zero. We accept any value providing that the error estimated for T_1 is within a specified range.

The most powerful aspect of FREDOM is the ability to follow the fate of individual voxels, and thus we usually acquire at least three baseline pO_2 maps, followed by further maps accompanying interventions, such as hyperoxic gas breathing. Even under baseline conditions, fluctuations in T_1 are apparent. These may arise from uncertainty in T_1, which may be reflected in $T_{1\,err}$ or transient fluctuations in pO_2.

T_1 map allows us to investigate sequential maps and select only those pixels that consistently show small $T_{1\,err}$s, for example, white regions of interest (ROI). In subsequent maps we may include only these regions, which satisfy the inclusion criteria for every map. This allows us to follow population dynamics based on specific tumor regions, avoiding potential anomalies due to varying numbers of "good quality" pixels in sequential images. Typically, 50–150 pixels provide high-quality data in any given map, but generally 20–80 pixels may be followed for a series of 23 maps associated with interventions.

The ROI tool also facilitates clustering, for example, selection of only those tumor regions, which consistently have $pO_2 < 10$ torr throughout the baseline period (these may be considered as chronically hypoxic, as opposed to regions, which fluctuate and may only be <10 torr in some

FIG. 7. Maps showing (A) ^{19}F NMR signal intensity, (B) spin–lattice relaxation times (T_1), (C) estimated errors in T_1, and (D) pO_2 values. Black squares show regions where signal to noise or data quality was so poor as to not provide a T_1 curve fit. Gray voxels show regions that provided a curve fit, but where the uncertainty in the data exceeded the threshold criteria (i.e., $T_{1\,err} > 2.5$ s or $T_{1\,err}/T_1 > 50\%$). All colored voxels ($n = 100$) provided a curve fit within the acceptance criteria in this map, but only those 56 voxels within the white regions of interest (ROI) provided consistently high-quality data throughout the sequence of eight maps acquired during baseline and with oxygen breathing. Data were obtained using the FREDOM approach from a representative Dunning prostate R3327-AT1 tumor (2 cm^3). (See color insert.)

baseline maps). The ability to follow groups of pixels with particular baseline characteristics has revealed heterogeneity in response to many interventions—often those regions initially well oxygenated show rapid and large response to hyperoxic gas breathing, whereas those that are initially poorly oxygenated show little and sluggish response (e.g., Fig. 8). This approach can also reveal phenomena such as the "steal" effect, whereby initially well-oxygenated regions decrease in pO_2, while others increase, which might appear as "no change," when histogram-based population statistics are used.

Figure 9 shows that the data quality is strongly related to signal amplitude. Although these data represent 56 voxels from a single tumor, we have previously shown similar data for the alternate PFC perflubron.[116] Given the high solubility of O_2 in PFCs, there could be a concern that PFCs act as reservoirs, perturbing local pO_2. Fig. 9B shows that there is no correlation ($r^2 < 0.05$) between signal amplitude (viz. HFB concentration) and pO_2.

As with any measurement, sampling is a critical issue. FREDOM is analogous to the Eppendorf Histograph in that it samples multiple locations, which appear to reflect interstitial pO_2. Histograph data suggest that a minimum of 100–140 data points[182] along five tracks[183] are required to accurately represent the pO_2 distribution of a tumor, though such criteria do depend on tumor size and heterogeneity. We applied Monte Carlo simulation to assess the data requirements for FREDOM. A data set was selected, which provided 120 high-quality data points, and these data points were accessed in random order with continuous calculation of mean pO_2 to assess the asymptotic trend lines toward the actual mean pO_2 (Fig. 10). It appears that about 50 data points are required to well represent the pO_2 distribution of the tumor, which is generally achievable in any individual pO_2 map. However, the unique ability to observe dynamic changes in pO_2 at multiple locations simultaneously is the greatest strength of FREDOM. Detection of heterogeneous responses is useful even if fewer data points are examined, since each location serves as its own control.

Validation of Measurements. The spin–lattice relaxation rate (R_1) is determined for each voxel using a three-parameter fit of signal intensities to

$$y_i = A[1 - (1 + W)\exp(-R_1 \times \tau)] \quad (4)$$

using the Levenberg–Marquardt least squares fitting protocol.[116] Typically, ~100–300 voxels provide an R_1 fit and potential pO_2 value. Because noise

[182] K. A. Yeh, S. Biade *et al.*, *Int. J. Radiat. Oncol. Biol. Phys.* **33**, 111 (1995).
[183] O. Thews, D. K. Kelleher *et al.*, *in* "Tumor Oxygenation" (P. W. Vaupel, D. K. Kelleher, and Günderoth, eds.), Vol. 24, p. 39. Gustav Fischer Verlag, Stuttgart, Germany, 1995.

A 21% O_2
B 21% O_2
C 100% O_2
D 95% O_2/5% CO_2
> 200
150
100
45
7
1 cm

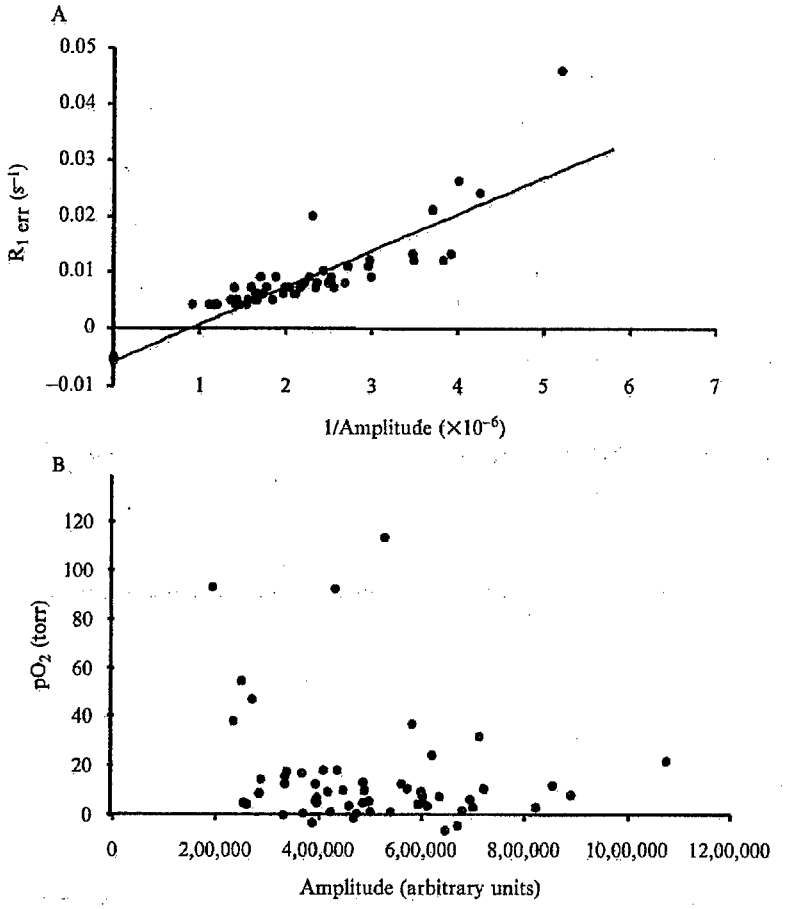

FIG. 9. (A) Relationship of $R_{1\ err}$ with signal amplitude showing strong correlation ($r^2 > 0.69$). (B) Relationship of pO_2 and signal amplitude showing lack of correlation ($r^2 < 0.05$).

FIG. 8. PO_2 maps obtained using the FREDOM approach from the tumor shown in Fig. 3. (A) Under baseline conditions, those voxels ($n = 56$) within the white region provided consistently reliable data during repeated measurements. (B) Baseline map (breathing air: $FO_2 = 21\%$): mean $pO_2 = 7.2 \pm 2.6$ (SE) torr, median $pO_2 = 1.3$ torr (range −7–88 torr). (C) Breathing oxygen ($FO_2 = 100\%$): fourth map obtained 24–32 min after switching from air: mean $pO_2 = 47.2 \pm 10.7$ torr ($p < 0.0001$ compared with baseline), median $pO_2 = 8.3$ torr (range −3–204 torr). (D) Breathing carbogen ($FO_2 = 95\%$): fifth map after switching to carbogen: mean $pO_2 = 43.1 \pm 9.2$ torr ($p < 0.0001$ compared with baseline), median $pO_2 = 5.6$ torr (range −10–216 torr). (See color insert.)

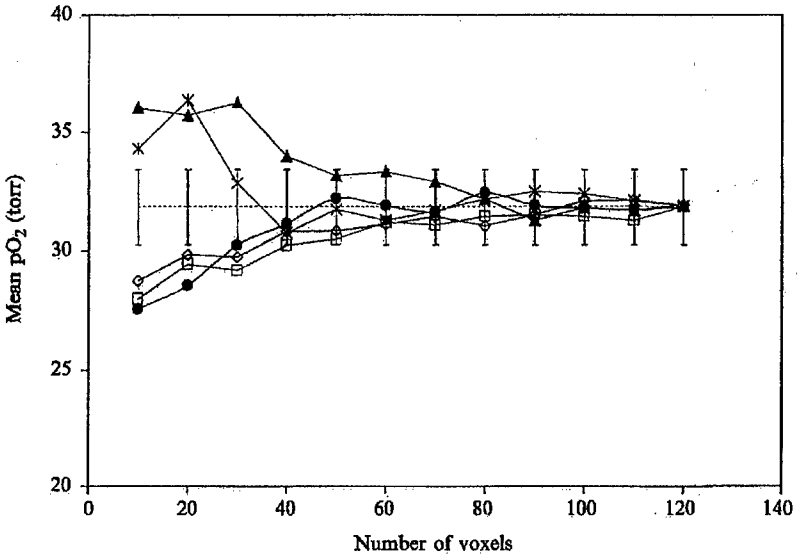

FIG. 10. Monte Carlo simulation of tumor oxygenation. Asymptotic behavior shows that tumor may be characterized by about 50 data points. For this large AT1 tumor in a rat breathing oxygen, all estimates converge on the mean $pO_2 = 31.7 + 1.0$ (SE) torr.

itself may give an apparent relaxation curve (R_1) fit, data are selected within a region of interest, having $T_{1\ err} < 2.5$ s and the ratio $T_{1\ err}/T_1 < 50\%$. With respect to respiratory interventions, only those voxels that provided consistently reliable data throughout the measurements are included for further analysis. At 37° and 4.7 T

$$pO_2(\text{torr}) = [R_1(s^{-1}) - 0.0835]/0.001876 \quad (5)$$

Equation (5) provides pO_2 in units of torr. The literature can be complicated by use of various units, and it may be instructive to provide conversion factors. We favor torr (1 torr = 1 mmHg), since radiobiologic hypoxia develops in the range 0–15 torr and this is the traditional unit favored by radiation biologists and oncologists. Further, 760 torr = 1 standard atmosphere (atm.), and gases are often quoted in %atm. For SI units, 101, 325 Pa (or N/m^2) = 1.01325×10^6 dynes/cm^2 = 1 atm. Some investigators quote oxygen concentrations in μM, often assuming that the solubility of oxygen in water at 37° is 1.35 μM/torr.[29] Quoting concentrations can be confusing because the solubility of oxygen is highly variable in solutions. FREDOM calibration is based on pO_2 values, and as shown by Eqs. 1–3,

these are directly related to the solubility of oxygen in HFB. However, partitioning of oxygen between the aqueous and PFC phases depends on pO_2, not concentrations. Thus the pO_2 determined by FREDOM will accurately reflect the ambient tissue pO_2 and if the solubility of oxygen can be estimated in the particular milieu, then $[O_2]$ could be calculated.

Both systematic and random errors may interfere. Random errors may be diminished by performing multiple repeat measurements (provided that the biologic system is stable). Systematic errors are more complex and could arise *inter alia* from erroneous calibrations, inappropriate curve fitting, and temperature changes. Appropriate curve fitting may be the greatest problem in relaxation analysis. Provided signal/noise > 10 for the most intense signals, we generally obtain excellent curve fits. Each voxel (or ROI) will comprise HFB at a range of pO_2 values, creating a multiexponential curve. However, modeling shows that the fit provides an "average" value. For population data, we sometimes determine error-weighted means $[\Sigma(x/\sigma^2)]/[\Sigma(1/\sigma^2)]$ in order to exploit as much available data as possible.

In terms of absolute pO_2 values, the most critical aspect is effective calibration curves. Over the years we have achieved pO_2-dependent ^{19}F NMR relaxation curves for many PFCs[116,141–143,160] and encountered potential pitfalls. The calibration curve we recommend at 4.7 T and 37° is given by Eq. (5) which was originally presented by Hunjan *et al.*[160] Briefly, 125 μl HFB was added to each of four gas-tight NMR tubes together with 0.5 ml water and saturated at 37° by bubbling with carbon dioxide, 1% O_2 (balance N_2), 9.8% O_2 (balance N_2), or air, respectively. Tubes were sealed, and the phantom was maintained at 37° in a water bath within a coil in the magnet. FREDOM was applied using the parameters described earlier, and the spin–lattice relaxation rates were estimated on a voxel-by-voxel basis using three-parameter fit. Equation (5) was established using linear regression analysis of amplitude squared weighted mean values for each gas.[159]

Although the relationship $R_1 = f(pO_2)$ is theoretically expected to be linear and empirically found to be so, we believe that it is important to use calibration gases in the range of physiologic pO_2. We recommend purchase of rigorously calibrated gases. We bubble gases for 30 min and use gas-tight Wilmad NMR tubes, which may be sealed with ground glass joints. Samples are used within hours of saturation. As desired, multiple tubes may be prepared at given pO_2, but since a linear relationship is expected, it may be equally appropriate to use additional gases. T_1 may be determined multiple times for each sample, and we recommend using the pulse sequence to be applied for *in vivo* investigations. In 1997, we published a calibration curve

$$R_1(s^{-1}) = 0.074(\pm 0.003) + 0.012(\pm 0.0002)pO_2(\%atm.) \quad (6)$$

for HFB at 37° and 4.7 T.[177] Considering temperature sensitivity gave

$$R_1(s^{-1}) = 0.77(\pm 0.03) - (0.00009 \pm 0.001)T(°C) + (0.018 \pm 0.003)P(\%atm.) - (0.00017 \pm 0.00008)TP(°C\%\ atm.) \quad (7)$$

More recently, we achieved Eq. (5) as a new calibration curve at 37° and 4.7 T using the ARDVARC approach.[160] This calibration curve is based on higher-quality data and provides superior pO_2 estimates. In particular, when tissue is expected to be hypoxic (excised tissue), we find fewer apparently negative pO_2 values.

A major strength of the FREDOM approach is that calibration curves remain valid between samples and across experimental platforms. Calibration curves obtained *in vitro* are valid *in vivo*. Thus we believe other investigators can apply Eq. (5) without the need to establish their own calibrations, provided that studies are undertaken at about 4.7 T and in the range 30–45°. As discussed in an earlier section and Table II, a 1° error in temperature estimates will only introduce a 0.13-torr error in pO_2 estimate, when pO_2 is about 5 torr. We also note that the calibration curves for HFB are relatively insensitive to magnetic field.[111,143]

We have previously investigated microbiodistribution of HFB based on Oil Red O stain, which indicated that HFB occurs as microscopic droplets (1–20 μm) widely distributed across tumor tissue.[175] Significantly, there was no evidence for formation of films, which could act as conduction conduits, causing oxygen equilibration. Occasionally, an animal (viz. tumor) will move slightly during a long time series of measurements. In this case the requirement of consistently high-quality curve fits throughout the data set for individual voxels fails because the tissues have moved relative to the voxel grid. Such motion is immediately apparent when examining the images. There is a choice of eliminating such a data set or relaxing the acceptance criteria and examining pO_2 population distribution without spatial continuity. It is important to recognize that all methods include a degree of sampling. In some approaches, this involves the selective placement and tracking of electrodes; in others, the choice of locations for biopsy and the number of microscopic fields of view. Sampling can be avoided by obtaining global measurements, as commonly acquired using near-infrared approaches, but this may itself mask the fundamental tumor heterogeneity[101] (see Chapter 17 in this volume).

We have previously shown that HFB shows little macroscopic redistribution over a period of hours.[177] It does clear from the tumors with a typical half-life of HFB of about 600 min, though some tumors show essentially no detectable clearance over a period of 6 h.[143,162] Clearance of HFB precludes long-term studies of chronic oxygenation, unless further doses of HFB are administered.

Comparison of pO_2 distributions using FREDOM or the Eppendorf Histograph has shown close similarity in both small and large tumors.[175] Dynamic studies in several tumor types have shown equivalent behavior when assessed using polarographic oxygen electrodes or OxyLite or FOXY optical probes.[32,43,134] Relative hypoxia has been compared with the histologic reporter pimonidazole, revealing similar trends across tumor types.[137]

Applications of FREDOM

FREDOM has been applied to investigations of diverse tumor types (syngeneic rat prostate and breast tumors and xenograft human lymphomas) with respect to growth and acute interventions.[27,32,134–137,160] Perhaps the greatest strength is the ability to investigate regional dynamic changes in pO_2 accompanying acute interventions. Figure 8 shows changes in regional pO_2 in an AT1 tumor accompanying hyperoxic gas breathing. As published previously,[137,160,162] the areas that were initially better oxygenated responded with elevated pO_2, whereas those relatively hypoxic regions showed little response. Data also may be presented as histograms (Fig. 11), revealing significant differences between mean and median pO_2 and hypoxic fractions between small and large tumors, and between the slow- and fast-growing sublines H and AT1 of the Dunning prostate R3327. Figure 12 shows variation in global mean pO_2 accompanying respiratory challenge with oxygen or carbogen and return to baseline following the intervention. Because individual tumor regions may be observed, local response may be compared at identical locations, efficiently comparing the efficacy of interventions (Fig. 13). Figure 14 shows the differential behavior of regions in undifferentiated Dunning prostate R3327-AT1 tumors versus highly differentiated H tumors. In each tumor type there are both well and poorly oxygenated regions under baseline conditions (see Fig. 11). In response to hyperoxic gas breathing, well-oxygenated regions in both tumor types show a rapid and significant elevation in pO_2, which is reversible when inhaled gas is returned to air (Fig. 14). Poorly oxygenated regions in H tumors respond slowly, but ultimately rise above the range of radiobiologic hypoxia, whereas corresponding regions in AT1 tumors do not. We also have investigated vasoactive drugs[42] and vascular targeting agents,[27] and the short-term changes in pO_2 following irradiation also have been examined.[184] Perhaps the most significant results to date

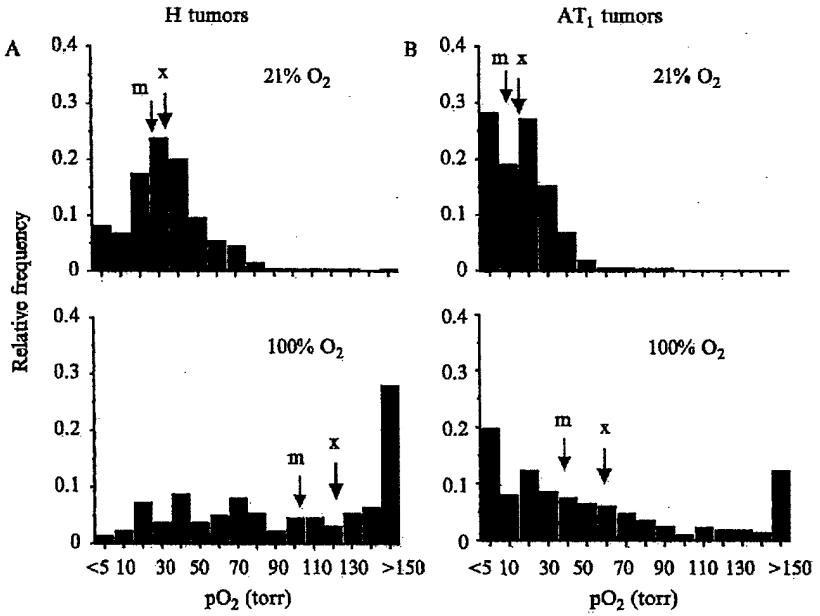

FIG. 11. Histograms of tumor oxygenation pooled for six H (A) and seven AT1 (B) small Dunning prostate R3327 rat tumors. The H tumors (219 voxels) showed significantly higher baseline pO_2 (mean = 31 ± 2 torr, median = 27 torr) than the size-matched AT1 tumors (338 voxels; mean = 14 ± 1 torr, median = 11 torr; $p < 0.0001$). With respect to oxygen challenge *(bottom)*, mean pO_2 in both groups increased significantly (mean = 122 ± 7 in the H versus, mean = 58 ± 4 in the AT1; $p < 0.0001$). Arrows indicate mean (x) and median (m) pO_2, respectively.

show that pO_2 measurements and detection of changes in pO_2 accompanying interventions correlate with the efficacy of tumor irradiation.[136]

Future

Ultimately, the value of a technique depends on its robustness, ease of use, and widespread implementation. To date, few laboratories had adopted the FREDOM approach because efficient investigation of HFB requires an unusual NMR pulse sequence. With the recent upgrade of our own instrumentation to the Varian Unity INOVA, the software is

[184] R. P. Mason, S. Hunjan *et al.*, *Int. J. Radiat. Oncol. Biol. Phys.* **42,** 747 (1998).

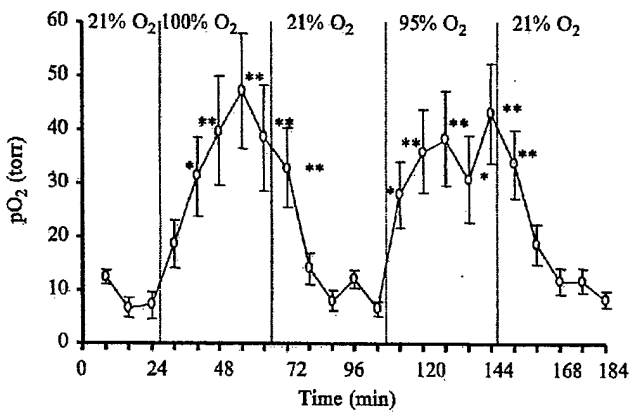

FIG. 12. Dynamic pO_2 (mean ± SE) obtained from sequential maps of the AT1 tumor shown in Fig. 8 with respect to respiratory challenge. *, $p < 0.001$; **, $p < 0.0001$ versus baseline.

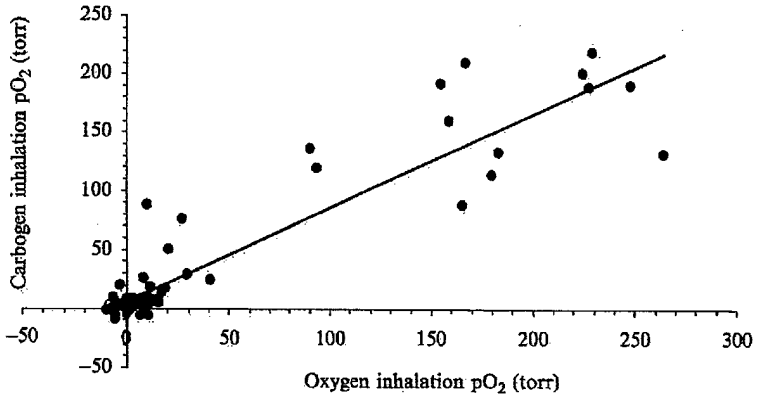

FIG. 13. Correlation between maximum pO_2 detected in each of 56 voxels from the AT1 tumor shown in Fig. 8, when the rat breathed oxygen versus carbogen ($r^2 > 0.85$).

now available on this popular platform, facilitating ready implementation elsewhere. In terms of research applications, it is known that tumor tissue pO_2 varies rapidly in response to many acute interventions, ranging from irradiation to photodynamic therapy, and various chemotherapies. We foresee FREDOM as a valuable tool for assessing the dynamic time course

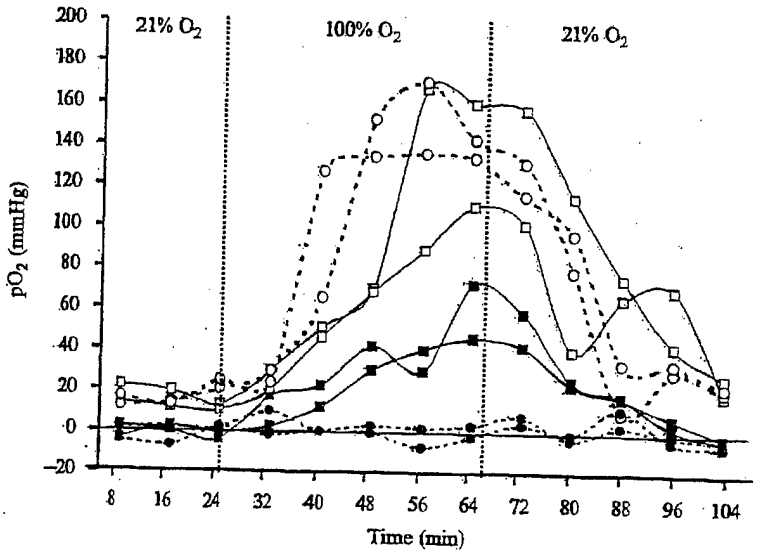

FIG. 14. Variation in pO_2 with respiratory challenge for individual regions chosen as initially well oxygenated ($pO_2 > 10$ torr) or hypoxic ($pO_2 < 5$ torr) from an AT1 (dotted lines) and H (solid lines) tumor, respectively. All the well-oxygenated regions in the two sublines increased significantly in pO_2 in response to oxygen breathing ($p < 0.01$). The hypoxic regions from the H tumor increased, whereas those in the AT1 tumor did not.

of such interventions to provide clear insight into the mode of action of therapeutic approaches and aid in the high-throughput screening of new drugs, such as vascular targeting and antiangiogenic agents.

Acknowledgments

This work was supported in part by NIH R01 CA79515 (NCI)/EB002762 (NIBIB), DOD Breast Cancer Initiative IDEA Award (DAMD 17–03–1–0363) (DZ) and predoctoral scholarship (DAMD 17–02–1–0592) (LJ) in conjunction with Cancer Imaging Program P20 CA 86354 and NIH BRTP Facility P41-RR02584. We are grateful to Dr. Anca Constantinescu for facilitating all the tumor investigations, Ms. Soon-Hee Sul for undertaking the Monte Carlo simulations, and Professor Eric Hahn for mentoring us in tumor biology.

Evaluation of breast tumor microcirculation and oxygenation using a combination of BOLD, DCE and 19F MRI

D. Zhao[1], L. Jiang[1], A. Constantinescu[1], E. W. Hahn[1], R. P. Mason[1]

[1]Radiology, UT Southwestern Medical Center, Dallas, TX, United States

Introduction: Tumor microcirculation and oxygenation play important roles in malignant progression and metastasis, as well as response to various therapies (1). Recognizing the intimate interplay of tumor oxygenation and blood flow, we have initiated investigations to compare regional changes in tissue pO_2 with vascularity. We have recently established a novel magnetic resonance approach to measuring regional tumor oxygen tension *FREDOM* (Fluorocarbon Relaxometry using Echo planar imaging for Dynamic Oxygen Mapping) with hexafluorobenzene, as the reporter molecule. This technique allows us to not only simultaneously examine multiple specific locations within a tumor, but also observe dynamic changes at individual locations with respect to intervention. Dynamic Contrast Enhanced (DCE) ^1H MRI based on exogenous Gd-DTPA and Blood Oxygen Level Dependent (BOLD) based on endogenous contrast deoxyhemoglobin are each sensitive to vascular characteristics. Here, we apply these MRI approaches to evaluate tumor oxygenation and vascularity and investigate the potential correlations among data set acquired by each technique.

Methods: Syngeneic breast NF13762 carcinomas were implanted in skin pedicles on the foreback of female Fisher rats. When the tumors reached ~ 1 cm diameter (Vol. ~ 0.6 cm^3), MR measurements were performed on a 4.7 T Varian system. Each rat was maintained under general anesthesia (air and 1% isoflurane). Hexafluorobenzene (50 µl) was injected into both central and peripheral regions in a single central plane of the tumor coronal to the rat's body. A tunable ($^1H/^{19}F$) single-turn solenoid coil (2 cm in diameter matched to the tumor size) was placed around the tumor-bearing pedicle. A single 2mm slice parallel to the rat body containing the strongest fluorine signal was chosen for the following ^1H DCE and BOLD and ^{19}F pO_2 studies. The transverse relaxation rate $R2^*$ was measured using multigradient echo sequence with 8 echoes (TR=195ms, TE=7ms and spacing =6ms) during air or oxygen breathing. After air equilibration, a series of spin echo planar images (constant recovery time τ = 500 ms (≡ TR) and TE=53 ms) obtained for BOLD response measurements during respiratory challenge. Following BOLD, the coil was retuned to ^{19}F. Tumor oxygenation was assessed on the same 2mm slice using ^{19}F PBSR-EPI of HFB with 6.5 minutes time resolution. A series of pO_2 maps was acquired over a period of 60 min with respiratory challenge, and corresponding regional pO_2 was estimated using the relationship: pO_2 (torr) = (R1-0.0836)/0.001876 (2). Finally, Dynamic Contrast Enhanced (DCE) MRI was performed on the 2mm slice using T1-weighted spin echo sequence (TR= 180ms, TE= 18ms) after a bolus injection of Gd-DTPA-BMA (0.1 mmol/kg, Omniscan) through a tail vein catheter. All data analysis was based on pixel by pixel basis.

Results: Each technique demonstrates intra-tumoral heterogeneity. As shown in Table 1, tumor pO_2 and BOLD SI increased and $R2^*$ decreased in response to respiratory challenge, and tumors with higher initial pO_2 and less hypoxic fraction (HF_{10}) had higher challenged pO_2 values ($r > 0.8$, $p < 0.01$). A significant correlation was found between ΔpO_2 and BOLD response ($r > 0.9$, $p < 0.001$, Fig. 1), while a lack of correlation between baseline pO_2 and the BOLD SI. There was no general correlation among pO_2, $R2^*$ and IAUC.

Table 1. Results of diverse MR approaches

Case	^{19}F pO_2 (torr)			BOLD	$R2^*$ (s^{-1})			DCE
no.	Air	HF_{10} (%)	Δ	(%)	Air	Oxygen	Δ	IAUC
1	36.3	0	136	14.1	46.1	42.6	-3.5	0.66
2	16.6	23	64.5	9.3	54.7	52.6	-2.1	1.00
3	12.5	31	49.6	7.5	69.4	63.8	-5.6	0.58
4	12.8	29	67.7	12.3	115.6	101.6	-14.0	0.49
5	11.5	33	21.5	2.9	64.1	66.7	2.6	0.40
6	12.3	21	19.8	2.3	49.9	47.6	-2.0	0.31
7	24.3	25	47.2	4.5	36.2	33.8	-2.4	0.61
8	NA	NA	NA	6.1	90.6	86.6	-4.0	0.87
Mean	18.0	23	58	7.4	65.8	61.9	-3.9	0.62

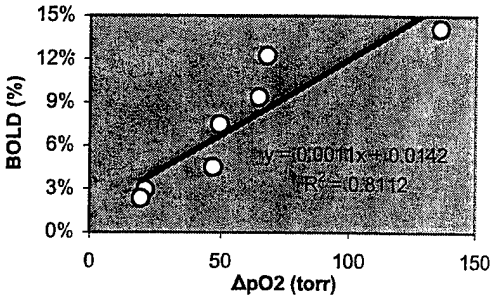

Fig.1. Correlation between ΔpO_2 and BOLD

Discussion: There is increasing evidence that tumor pO_2 has prognostic value in the clinic (1). Using the *FREDOM* approach we are able to detect intra-tumor differences in oxygenation. One might anticipate that non-invasive vascular dynamics could provide surrogate markers for tumor oxygenation. While we have found that BOLD and DCE provide a qualitative indication of tumor vascular dynamics, our results suggest a lack of correlation with tumor pO_2 itself. However, there was a strong correlation between BOLD response and ΔpO_2 accompanying oxygen challenge.

References:

1. Höckel, M., Vaupel, P., *J. Natl. Cancer Inst.*, 93, 266-276, 2001.
2. Hunjan, S., Zhao, D., Constantinescu, A., Hahn, E.W., Antich, P.P., Mason, R.P., *Int. J. Radiat. Oncol. Biol. Phys.*, 49, 1097-1108, 2001.

Acknowledgment: Supported by DOD Breast Cancer DAMD 170310363 and NCI RO1 EB2762 and P20 CA86354.

REFERENCE #: ZHA-1074-274136

Interrogation of tumor vasculature and oxygenation by integrated ^{1}H and ^{19}F MRI

AUTHORS:

Dawen Zhao [1]
Dallas, TX 75390 US[1]
Lan Jiang [1]
Dallas, TX 75390 US[1]
Anca Constantinescu [1]
Dallas, TX 75390 US[1]
Eric Hahn [1]
Dallas, TX 75390 US[1]
Ralph Mason [1]
Dallas, TX 75390 US[1]

ABSTRACT:

Tumor oxygenation has been widely recognized as a potent factor influencing tumor response to various therapies, especially radiotherapy. Recognizing the intimate interplay of tumor oxygenation and vascularization, we have initiated investigations to compare regional changes in tissue pO_2 with vascularity in syngeneic breast NF13762 carcinomas by integrated ^{1}H and ^{19}F MRI. Tissue pO_2 dynamics were assessed using FREDOM (Fluorocarbon Relaxometry using Echo planar imaging for Dynamic Oxygen Mapping) with hexafluorobenzene, as the reporter molecule. Dynamic Contrast Enhanced (DCE) ^{1}H MRI based on exogenous Gd-DTPA and Blood Oxygen Level Dependent (BOLD) ^{1}H MRI based on endogenous contrast deoxyhemoglobin were used to interrogate vascular characteristics. FREDOM revealed considerable intra tumoral heterogeneity in the distribution of pO_2 values. A mean pO_2 increased significantly from a baseline 18 ±4 (se) torr to a maximum value 78 ±16 torr and a mean HF<10 mmHg decreased from 23 % to 4 %, in response to oxygen breathing. The increase in tissue pO_2 (ΔpO_2) correlated closely with BOLD response to oxygen ($r > 0.9$, $p < 0.001$). However, DCE MRI data (IAUC) showed no correlation with ^{19}F pO_2 or BOLD data. The non-invasive BOLD and DCE MRI are capable of qualitatively measuring blood oxygenation and perfusion. Combination with information on quantitative tissue oxygenation by ^{19}F MR will provide better understanding of tumor physiology and response to intervention. *Supported by DOD Breast Cancer DAMD 170310363 and NCI RO1 EB2762 and P20 CA86354.*

KEYWORDS:

vasculature, Tumor hypoxia, ^{1}H MRI, ^{19}FMRI